

Proteome-wide Dysregulation by PRA1 Depletion Delineates a Role of PRA1 in Lipid Transport and Cell Migration*[§]

Hao-Ping Liu[‡], Chih-Ching Wu^{‡§}, Hung-Yi Kao[‡], Yi-Chuan Huang[‡], Ying Liang[‡], Chia-Chun Chen[¶], Jau-Song Yu^{‡||}, and Yu-Sun Chang^{¶**}

We have previously identified prenylated Rab acceptor 1 (PRA1) as a novel cellular interacting partner for Epstein-Barr virus-encoded oncoprotein, latent membrane protein 1 (LMP1). The intracellular trafficking and full signaling of LMP1 requires its interaction with PRA1. To further explore the role of PRA1 in Epstein-Barr virus-associated nasopharyngeal carcinoma (NPC) cells, we generated several PRA1-knockdown cell clones, which exhibited altered cell morphology and increased cell motility. We identified proteins differentially expressed in the knockdown clones by means of isobaric mass tags labeling coupled with multidimensional liquid chromatography-mass spectrometry. We validated a panel of proteins, which showed consistent up-regulation in PRA1-knockdown clones and participated in regulating lipid homeostasis and cell migration. Immunofluorescence staining further revealed altered localization of these proteins and accumulation of intracellular cholesterol in PRA1-knockdown clones. These effects were phenocopied by treatment with a cholesterol transport inhibitor, U18666A. Moreover, overexpressed PRA1 was able to alleviate the dysregulation of these affected proteins either from PRA1 knockdown or U18666A treatment, implying a role for PRA1 in regulating the levels of these affected proteins in response to altered cholesterol homeostasis. We further demonstrated that LMP1 expression caused PRA1 sequestration in NPC cells, leading to a consequence reminiscent of PRA1 knockdown. Finally, the immunohistochemistry showed a physiological relevance of the PRA1-associated proteome-wide changes in NPC biopsy tissues. In sum, our findings delineated novel roles of PRA1 in lipid transport and cell migration, and provided additional insights into the molecular basis of NPC morphogenesis, namely a consequence of LMP1-PRA1 interaction. *Molecular & Cellular Proteomics* 10:10.1074/mcp.M900641-MCP200, 1–19, 2011.

From the [‡]Molecular Medicine Research Center, [§]Department of Medical Biotechnology and Laboratory Science, [¶]Graduate Institute of Biomedical Sciences, and ^{||}Department of Cell and Molecular Biology, Chang Gung University, Tao-Yuan 333, Taiwan

Received December 30, 2009, and in revised form, March 30, 2010

Published, MCP Papers in Press, June 30, 2010, DOI 10.1074/mcp.M900641-MCP200

Prenylated Rab acceptor 1 (PRA1)¹, which is a transmembrane protein of 21 kDa, is ubiquitously expressed in human tissues and localizes at the Golgi apparatus, post-Golgi vesicles, endosomes, and the plasma membrane (1, 2). As revealed by its name, PRA1 interacts with numerous Rab GTPases (2, 3), the latter of which function in a wide variety of biological processes such as endocytosis and exocytosis and have emerging roles in diseases (4–6). The PRA1-Rab interactions may assist in the packaging of Rabs into vesicles for transport to the destined compartments (2). Moreover, PRA1 also acts as a dual receptor for vesicle-associated membrane protein 2 (VAMP2) and GDP dissociation inhibitor 1 (GDI1) (7, 8). As a GDI displacement factor, PRA1 is able to catalytically dissociate endosomal Rabs (Rab9 and Rab5) from GDI-bound complexes and thereby escorts the liberated Rabs onto membranes (9). Given this relative lack of Rab specificity, PRA1-mediated regulation of Rab proteins is probably restricted by the cellular localization of PRA1, *i.e.* PRA1 regulates the Rabs present in the organelles with which PRA1 associates.

Although its precise physical role remains to be better elucidated, PRA1 seems to function in the regulation of docking and fusion of transport vesicles both in the Golgi apparatus and at the plasma membrane, or alternately function as a sorting protein in the Golgi apparatus (10). PRA1 can form a complex with Rab3a and VAMP2, and the interaction of this complex can result in VAMP2 activation (7). Once activated, VAMP2 interacts with syntaxin, followed by the docking and fusion of transport vesicles with target membrane (11). Since syntaxin and VAMP2 are enriched in Golgi-derived lipid rafts (12), PRA1 is thought to associate with lipid rafts (13).

As a platform for lipid-lipid and lipid-protein interactions, lipid rafts play critical roles in protein transport, sorting, targeting, signaling as well as membrane trafficking, and are

¹ The abbreviations used are: PRA1, prenylated rab acceptor 1; CAV1, caveolin-1; EBV, Epstein-Barr virus; FABP5, fatty acid-binding protein, epidermal; GDI, GDP dissociation inhibitor 1; ITGA6, integrin alpha-6; ITGB4, integrin beta-4; iTRAQ, isobaric tags for relative and absolute quantitation; LC, liquid chromatography; LAMC2, laminin subunit gamma-2; LMP1, latent membrane protein 1; MPR, mannose 6-phosphate receptor; NPC, nasopharyngeal carcinoma; MS/MS, tandem mass spectrometry; PFIN2, profilin-2; TIP47, tail-interacting protein of 47 kDa; VAMP2, vesicle-associated membrane protein 2.

essential for enveloped virus budding and assembly (14). In agreement with this notion, several viral proteins have been shown to interact with PRA1 to benefit the survival of viruses. For instance, the spike protein VP4 encoded by rotavirus and the envelope transmembrane protein gp41 encoded by retrovirus can interact with PRA1, and their interaction with PRA1 may in turn enhance the assembly of rotavirus and retrovirus particles, respectively (13, 15). In this regard, it is conceivable to speculate a role for PRA1 in promoting or stabilizing protein association with lipid rafts.

In the previous study, we have identified PRA1 as a novel binding partner for the Epstein-Barr virus (EBV)-encoded oncoprotein, latent membrane protein 1 (LMP1) (16). EBV is closely associated with human diseases including nasopharyngeal carcinoma (NPC) (17), which is one of the common cancers in Taiwan and southern China, and LMP1 is shown to mainly contribute to these EBV-associated malignancies (18). By mimicking members of tumor necrosis factor receptor (TNFR) family, LMP1 can induce several signaling pathways in a constitutively-activated manner to exert its oncogenic potency (19–21). Importantly, the intracellular trafficking of LMP1 requires its interaction with PRA1, and this requirement is critical for full activation of LMP1-mediated signaling (16). Accordingly, delineating the propensity of PRA would shed light on the nature of PRA1-LMP1 interaction and yield additional insights into the tumorigenesis of NPC.

To further assess the role of PRA1 in NPC cells, in this study we generated several PRA1-knockdown NPC cell clones, which displayed altered cell morphology, and used these clones to analyze the effect of PRA1 on cell morphology and relevant biological processes. We discovered a panel of dysregulated proteins in PRA1-knockdown clones, which participate in lipid metabolism and transport and cell adhesion and migration, by using isobaric mass tags (iTRAQ) labeling approaches combined with multidimensional liquid chromatography-mass spectrometry (LC-MS/MS). To determine the physiological relevancy of our findings, we investigated the functional consequence of PRA1 sequestration in LMP1-expressing cells. We confirmed the phenotype of LMP1-expressing cells, namely intracellular cholesterol accumulation, elevated expression levels of those PRA1-affected proteins, and increased cell motility, consistent with the effect of PRA1 knockdown. We also validated the PRA1-associated dysregulation of selected proteins in NPC tissues using immunohistochemistry.

Taken together, our findings revealed a PRA1-involved modulation in lipid homeostasis and cell migration, and implied an unexpected association of the LMP1-PRA1 interaction with NPC morphogenesis.

EXPERIMENTAL PROCEDURES

Antibodies—The polyclonal antibody against human PRA1 was generated as previously described (16). The anti-LMP1 monoclonal antibody (S12) was affinity purified from hybridoma. The monoclonal antibody specific to integrin $\alpha 6$ (ITGA6), ITGB4, LAMC2, or FABP5, and polyclonal antibody against CAV1, calreticulin or TIP47 were

purchased from Santa Cruz (Santa Cruz, CA). The monoclonal antibody specific to PFN2, and polyclonal antibody against annexin A3 were purchased from Abcam (Cambridge, UK). fluorescein isothiocyanate-conjugated anti-ITGA6 and PE-conjugated anti-ITGB4 monoclonal antibodies, and fluorescein isothiocyanate- or tetramethyl rhodamine iso-thiocyanate-conjugated secondary antibodies were purchased from BD Transduction Laboratories (BD Biosciences).

Cell Culture—NPC-TW04 cells were cultured at 37 °C and 5% CO₂ in Dulbecco's modified Eagle's media supplemented with 10% fetal calf serum, penicillin, and streptomycin. NPC cells stably expressing LMP1 were established previously (22) and cultured in Dulbecco's modified Eagle's media with 10% fetal calf serum and 200 μ g/ml G418. Where indicated, cells were incubated with 3 μ M U18666A (Sigma-Aldrich) for 20 h prior to harvesting.

PRA1-knockdown Stable Clones—PRA1 shRNA (nucleotides 319–337) was designed as previously described (16). The oligoduplexes were cloned into pSUPER-puro (Oligoengine), and transfected into NPC-TW04 cells using Lipofectamine (Invitrogen). Twenty-four hours later, transfected cells were selected for 14 days with 1 μ g/ml puromycin. Pooled populations of knockdown cells were further subcloned and maintained under puromycin selection. Control cell lines were generated by transfecting cells with a pSUPER-puro construct, which did not yield any appreciable knockdown of the protein product in Western blot analysis.

Preparation of Cell Extracts and Digestion of Protein Mixtures—Cell extracts were prepared as previously described (23). Briefly, two PRA1-knockdown NPC cell clones and two control clones were washed three times with 10 ml of PBS, lysed in hypotonic buffer (10 mM Tris, pH 7.4, 1 mM EDTA, 1 mM EGTA, 50 mM NaCl, 50 mM NaF, 20 mM Na₄P₂O₇, 1 mM Na₃VO₄, 1 mM phenylmethylsulfonyl fluoride, 1 mM benzamidine, 0.5 μ g/ml leupeptin, and 1% Triton-X100) on ice for 15 min. The cell lysates of four samples were collected in parallel and then sonicated on ice, followed by centrifugation at 10,000 \times g for 25 min at 4 °C. The resulting supernatants were used as the cell extracts. Protein concentrations were determined by the BCA protein assay reagent from Pierce (Rockford, IL, USA). For tryptic in-solution digestion, the protein mixtures were denatured with 8 M urea containing 50 mM triethylammonium bicarbonate (Sigma-Aldrich), reduced with 10 mM Tris(2-carboxyethyl)-phosphine (Sigma-Aldrich) at 37 °C for 90 min, and then alkylated with 10 mM methyl methanethiosulfonate (Sigma-Aldrich) at room temperature for 20 min. After desalting, the protein mixtures were in-solution digested with modified, sequencing grade trypsin (Promega, Madison, WI) at 37 °C overnight.

iTRAQ Reagent Labeling and Fractionation by Strong Cation Exchange (SCX) Chromatography—The peptides were labeled with the iTRAQ reagent (Applied Biosystems, Foster City, CA) according to the manufacturer's protocol. Briefly, one unit of label (defined as the amount of reagent required to label 100 μ g of protein) was thawed and reconstituted in ethanol (70 μ l). The peptide mixtures were reconstituted with 25 μ l iTRAQ dissolution buffer. The aliquots of iTRAQ 114, 115, 116, and 117 were combined with peptide mixtures from the two control samples (C15, C15–3) and two PRA1-knockdown samples (K3–2, K3–14), respectively, and incubated at room temperature for 1 h. The peptide mixtures were then pooled, dried by vacuum centrifugation. The dried peptide mixture was reconstituted and acidified with 0.5 ml buffer A (0.1% formic acid and 25% acetonitrile, pH 2.5) for fractionation by SCX chromatography using the Ettan MDLC system (GE Healthcare).

For peptide fractionation, the iTRAQ-labeled peptides were loaded onto a 2.1 mm \times 250 mm BioBasic SCX column containing 5- μ m particles with 300- μ m pore size (Thermo Electron). The peptides were eluted at a flow rate of 100 μ l/min with a gradient of 0%–10% buffer B (300 mM NH₄Cl, 0.1% formic acid and 25% acetonitrile, pH 2.5) for

20 min, 10–20% buffer B for 35 min, 20%–50% buffer B for 15 min, and 50%–100% buffer B for 10 min. The elution was monitored by absorbance at 220 nm, and fractions were collected every 1 min. Each fraction was vacuum dried and then resuspended in 0.1% formic acid (20 μ l) for further desalting and concentration using the ziptip home-packed with C18 resin (5–20 μ m, LiChroprep RP-18, Merck, Taipei, Taiwan).

Liquid Chromatography (LC)-Electrospray Ionization (ESI) Tandem MS (MS/MS) Analysis by LTQ-Orbitrap PQD—To analyze the iTRAQ-labeled peptide mixtures, each peptide fraction was reconstituted in high performance liquid chromatography (HPLC) buffer A (0.1% formic acid), loaded across a trap column (Zorbax 300SB-C18, 0.3 \times 5 mm, Agilent Technologies, Wilmington, DE) at a flow rate of 0.2 μ l/min in HPLC buffer A, and separated on a resolving 10-cm analytical C₁₈ column (inner diameter, 75 μ m) with a 15- μ m tip (New Objective, Woburn, MA). The peptides were eluted using a linear gradient of 2%–30% HPLC buffer B (99.9% acetonitrile containing 0.1% formic acid) for 63 min, 30%–45% buffer B for 5 min, and 45%–95% buffer B for 2 min with a flow rate of 0.25 μ l/min across the analytical column.

The LC setup was coupled on line to a linear ion trap mass spectrometer linear trap quadrupole (LTQ)-Orbitrap (Thermo Fisher, San Jose, CA) operated using the Xcalibur 2.0 software (Thermo Fisher). Intact peptides were detected in the Orbitrap at a resolution of 30,000. Internal calibration was performed using the ion signal of (Si(CH₃)₂O)₆H⁺ at *m/z* 445.120025 as a lock mass (24). Peptides were selected for MS/MS using pulsed Q collision induced dissociation (PQD) operating mode with a normalized collision energy setting of 27% and fragment ions were detected in the LTQ (25, 26). The data-dependent procedure that alternated between one MS scan followed by three MS/MS scans for the three most abundant precursor ions in the MS survey scan was applied. The *m/z* values selected for MS/MS were dynamically excluded for 180 s. The electrospray voltage applied was 1.8 kV. Both MS and MS/MS spectra were acquired using the 4 microscan with a maximum fill-time of 1000 and 100 ms for MS and MS/MS analysis, respectively. Automatic gain control was used to prevent over-filling of the ion trap, and 5 \times 10⁴ ions were accumulated in the ion trap for generation of PQD spectra. For MS scans, the *m/z* scan range was 350 to 2,000 Da.

Sequence Database Searching and Data Analysis—MS/MS spectra were searched using MASCOT engine (Matrix Science, London, UK; version 2.2.04) against a nonredundant International Protein Index human sequence database v3.27 (released at March 2007; 67,528 sequences; 28,353,548 residues) from the European Bioinformatics Institute (<http://www.ebi.ac.uk/>). For protein identification, 10 ppm mass tolerance was permitted for intact peptide masses and 0.5 Da for PQD fragment ions, with allowance for two missed cleavages made from the trypsin digest, oxidized methionine (+16 Da) as a potential variable modification, and iTRAQ (N-terminal, +144 Da), iTRAQ (K, +144 Da), and MMTS (C, +46 Da) as the fixed modifications.

The MASCOT search results for each SCX elution were further processed using the Trans-Proteomic Pipeline (TPP, version 3.4), which includes the programs PeptideProphet, ProteinProphet, and Libra (27, 28). PeptideProphet, a peptide probability score program, aids in the assignment of peptide MS spectrum (29). ProteinProphet program assigns and groups peptides to a unique protein or a protein family if the peptide is shared among several isoforms, and allows filtering of large scale data sets with assessment of predictable sensitivity and false positive identification error rates (30). We used the ProteinProphet probability score \geq 0.95 to ensure an overall false positive rate below 1%, and excluded the protein identified with single peptide hit. Protein quantification was achieved with the Libra program (28, 31), and the default setting of Libra was used. A weighted average of the peptide iTRAQ ratios per protein was used to

quantify the protein. Peptide with iTRAQ reporter ion intensities lower than 30 was removed to improve the reliability of protein quantification; peptide with an iTRAQ ratio beyond twofold deviation from the mean ratio was also excluded as an outlier. A 1.23-fold change cutoff for all iTRAQ ratios (ratio <0.80 or >1.23) was selected to classify proteins as up- or down-regulated. Proteins with iTRAQ ratios below the low range (0.80) were considered to be under-expressed, whereas those above the high range (1.23) were considered overexpressed. Information about the PeptideProphet, ProteinProphet, and Libra programs in the TPP can be accessed from Institute for Systems Biology of the Seattle Proteome Center (<http://www.proteomecenter.org/>).

RNA Interference—NPC-TW04 cells were transfected with 50 nm dsRNA duplexes and 50 μ l Lipofectamine™ 2000 (Invitrogen) according to the manufacturer's protocol. SMARTpool reagents including four 21-bp RNA duplexes targeting PRA1 sequence were purchased from Dharmacon (Lafayette, CO). The oligonucleotide sequences are presented as follows: pool duplex 1, sense 5'-GCAACUAUGUGUU-CGUGUUUU and antisense 5'-PAACACGAACACAUAGUUGCUU; pool duplex 2, sense 5'-GCAGAUGGAACCCGUGUGAUU and antisense 5'-PUCACACGGUCCAUCUGCUU; pool duplex 3, sense 5'-GCAGAAAGAUGCCGAGGCGUU and antisense 5'-PCGCCUCG-GCAUCUUUCUGCUU; pool duplex 4, sense 5'-CCUGUUAUACUUCU-AUCUUU and antisense 5'-PAGAUAGAGAAUGUACAGGUU. Control siRNA was synthesized by Research Biolabs (Ayer Rajah Industrial Estate, Singapore). At 72 h post-transfection, cells were harvested, and cell extracts were prepared for Western blotting to confirm the knockdown efficacy.

Subcellular Fractionation—Approximately 80% confluent cells were washed twice in PBS and scraped into Bud buffer (38 mM potassium aspartate, 38 mM potassium glutamate, 38 mM potassium gluconate, 20 mM potassium MOPS, pH 7.2, 5 mM sodium carbonate, 2.5 mM magnesium sulfate, 2 mM EGTA, 5 mM reduced glutathione, adjusted to pH 7.2 with KOH) with freshly added protease inhibitors. A cytoplasmic extract was prepared by homogenization with 10 strokes in a cell homogenizer and then centrifuged at 800 \times *g* for 10 min. The resultant supernatant was layered onto a continuous sucrose gradient (10%–45% sucrose in MOPS buffer containing 20 mM EGTA) and centrifuged at 50,000 rpm in a SW50.1 rotor (Beckman, Fullerton, CA) for 3 h. The fractions were collected manually from the top of the gradient, and an equal portion of each fraction was subjected to Western blot analysis.

Western Blot Analysis—Whole-cell lysates were homogenized and lysed in a buffer containing 50 mM Tris-Cl (pH 7.5), 150 mM NaCl, 10 mM MgCl₂, 1 mM ethylenediamine tetraacetate (pH 8.0), 1% Nonidet P-40, 100 mM sodium fluoride, 1 mM phenylmethanesulfonyl fluoride, and 2 μ l/ml protease inhibitor mixture (Sigma-Aldrich). Protein concentrations were determined using the protein assay reagent (Bio-Rad), and equal amounts of proteins (30–50 μ g/lane) were resolved on 12% sodium dodecyl sulfate (SDS)-polyacrylamide gel. The proteins were then electro-transferred onto nitrocellulose membranes (Amersham Biosciences). After blocking with 5% nonfat powdered milk in TBS, blots were incubated with the respective primary antibodies at 4 °C overnight. Membranes were incubated with the respective secondary antibody, horseradish peroxidase-conjugated rabbit/goat/mouse anti-IgG (Invitrogen) for 1 h at room temperature. Protein bands were detected by the enhanced chemiluminescence method (Pierce® ECL, Thermo Scientific) on Fuji SuperRx films.

Immunofluorescence Microscopy—Cells grown on polylysine-coated coverslips were fixed with 4% formaldehyde, permeabilized and blocked with 0.1% saponin containing 1% bovine serum albumin for 20 min. The coverslips were incubated with the indicated primary antibodies for 2 h, followed by incubation with the appropriate fluorophore-conjugated secondary antibodies for 45 min at room temperature. Nuclei were stained with 4'-6-diamidino-2-phenylindole

(Sigma-Aldrich). For intracellular cholesterol staining, coverslips were incubated in 50 $\mu\text{g/ml}$ filipin (Sigma-Aldrich) for 1 h after fixation. All coverslips were mounted with the VECTASHEILD reagent (Vector Laboratories Inc., CA, USA) and visualized by confocal microscopy using a ZEISS LSM510 META laser scanning microscope (Carl Zeiss, Germany) with a 63×1.32 NA oil immersion objective.

Clinical Specimens—Tumor specimens for immunohistochemistry were collected from 10 NPC patients (five nonkeratinizing cancers and five undifferentiated cancers) at the Department of Otolaryngology-Head and Neck Surgery, Chang Gung Memorial Hospital (Lin-Kou, Taiwan, Republic of China) from 2002 to 2003. These included two stage-II, four stage-III, and four stage-IV patients comprising seven men and three women ranging from 22 to 78 years of age (mean age 39.5). The study protocol was approved by the Medical Ethics and Human Clinical Trial Committee at Chang Gung Memorial Hospital. All patients entered in the study signed an informed consent.

Immunohistochemistry—Samples of NPC tissue and adjacent normal nasopharynx tissue were obtained from patients undergoing surgery and were frozen immediately after surgical resection. Immunohistochemistry was performed according to the previously described procedures (32). Staining for LMP1, PRA1, CAV1, ITGA6, ITGB4, or LAMC2 was carried out using the Envision-kit (DAKO, Carpinteria, CA). Briefly, the sections were deparaffinized with xylene, dehydrated with ethanol and then heated in 0.01 M citrate buffer (pH 6.0). Endogenous peroxidase activities were inactivated in 3% H_2O_2 for 10 min at room temperature, and the sections were blocked with 3% normal goat serum in 0.2 M PBS (pH 7.4). Samples were then incubated with antibodies specific for proteins described above for 2 h at room temperature. Secondary antibody-coated polymer peroxidase complexes (DAKO) were then applied for 30 min at room temperature, followed by treatment with substrate and chromogen (DAKO) and a further incubation for 5–10 min at room temperature. Slides were counterstained with hematoxylin. Expression of the individual protein was evaluated according to the simplified H score system (33), which is based on the percentage of cell staining: 3 ($\geq 90\%$), 2 (50%–89%), 1 (10%–49%), or 0 (0%–9%), and the intensity of cell staining: 3 (high), 2 (moderate), 1 (low), or 0 (no cell staining). The two scores were multiplied by each other and then divided by three to get the final score. Strong staining was defined as a final score >2 , moderate staining was defined as a final score >1 , and weak staining was defined as a final score ≤ 1 .

Supplementary Data—The Supplementary Data are available at *Molecular and Cellular Proteomics* online (<http://www.mcponline.org>).

RESULTS

Morphological Changes in PRA1-knockdown Cells—To investigate the function of PRA1 in NPC cells, we generated several PRA1-knockdown clones by persistent expression of PRA1 shRNA in NPC cells. When grown at a low cell density, the PRA1-knockdown cells exhibited a sparse distribution and fibroblast-like shape, in contrast to the epithelial morphology of control cells showing a relatively tighter cell-cell contact (Fig. 1A). These PRA1-knockdown cells also exhibited increased cell motility as revealed in wound healing assays (Fig. 1B), in which wounds made in PRA1-knockdown cells were completely healed by 16 h postwounding compared with the controls healed by 24 h (data not shown). No significant change in the cell proliferation rate was observed between control and PRA1-knockdown cells (Supplementary Fig. S1A). The knockdown efficacy (exceeding 80% reduction) was val-

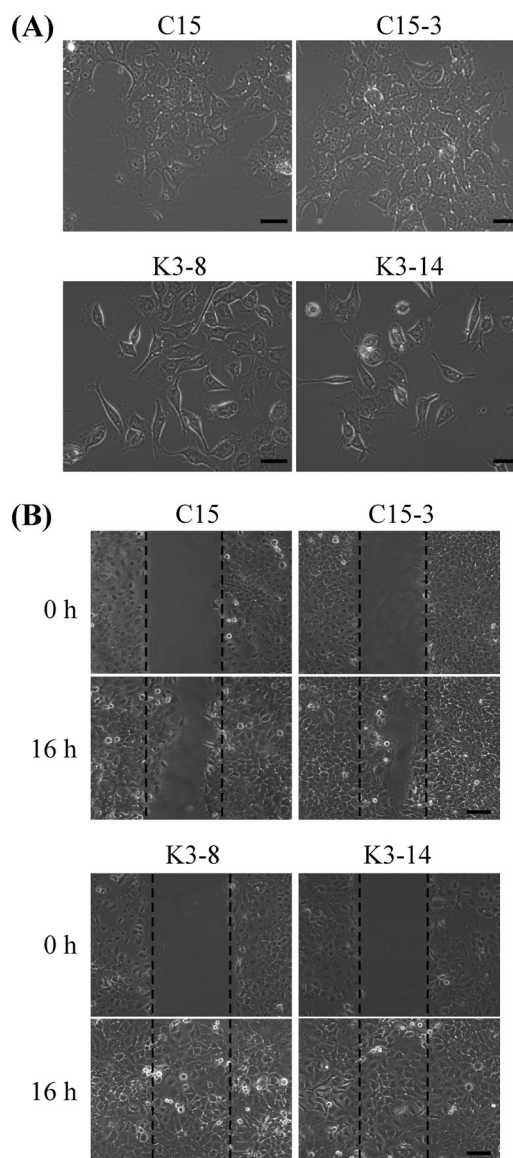


Fig. 1. Altered cell morphology and increased cell motility of PRA1-knockdown cell clones. A, PRA1-knockdown clones (K3-2, K3-14) exhibited elongated and fibroblast-like shape when grown at subconfluence, whereas control clones (C15, C15-3) showed epithelial morphology with relatively strong cell-cell contacts. Scale bar, 100 μm . B, A wound healing assay was performed to track cell migration of two PRA1-knockdown clones and two control clones. Cells were seeded in 60-mm plates at high density and allowed to form monolayers overnight. After wounding with a pipette tip, the wound healing activity was observable between 3 and 24 h. By 16 h, cell migration could be easily differentiated between cells with a low magnification (10 \times) objective. Scale bar, 100 μm .

idated by real-time RT-PCR (Supplementary Fig. S1B) and Western blot analysis (Fig. 2A).

Identification of Proteins Differentially Expressed in PRA1-knockdown Cells by iTRAQ-LC-MS/MS Analysis—We then sought to analyze the morphological changes of PRA1-knockdown cells in the aspect of protein expression. To identify

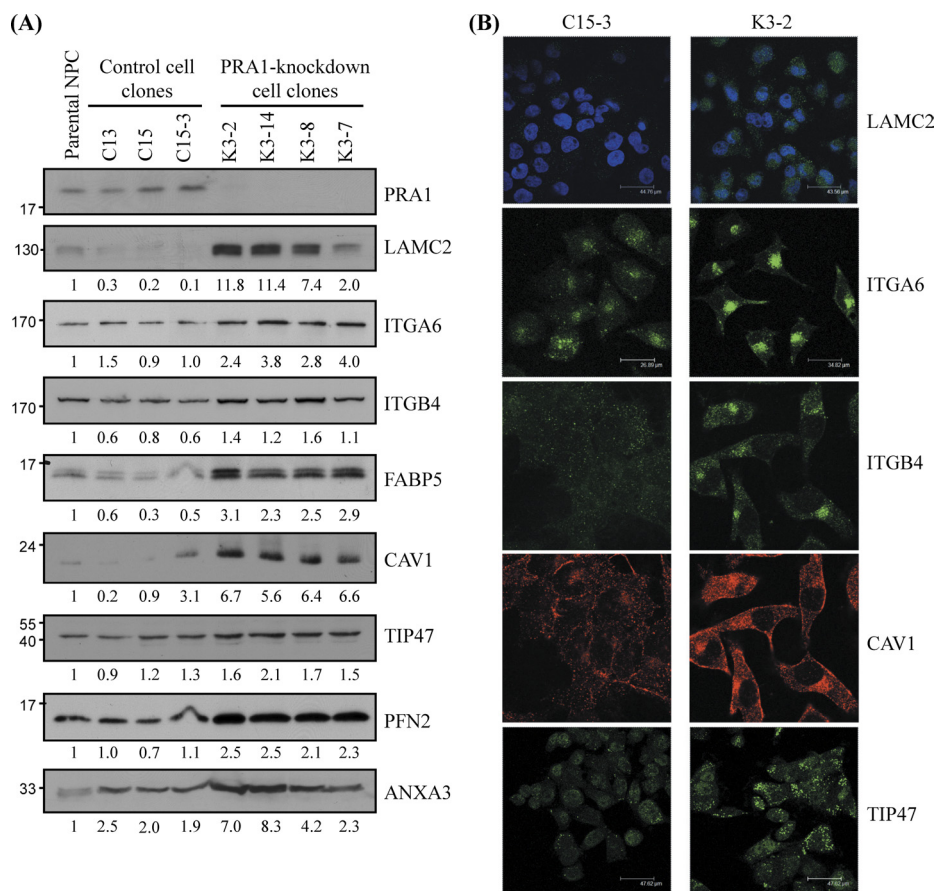


FIG. 2. Validation of the protein levels of selected candidates discovered by iTRAQ in PRA1-knockdown cell clones. *A*, Equal amounts of protein lysates individually from four PRA1-knockdown clones (K3-2, K3-7, K3-8, and K3-14), three control clones (C15, C15-1, and C15-3), and parental NPC-TW04 cells (NPC) were applied to Western blot analysis using antibodies as indicated. α -tubulin was used as a loading control. Numbers represent relative fold differences of protein levels on the basis of densitometer quantitation. *B*, Immunofluorescent staining for PRA1-affected proteins in NPC cells. Cells from each of two PRA1-knockdown clones (K3-2, K3-8) or each of two control clones (C15, C15-3) were grown on coverslips for 48 h, then fixed and probed with specific antibodies as indicated, followed by incubation with corresponding fluorophore-conjugated secondary antibodies and acquisition of images as detailed under “Experimental Procedures.” Intracellular LAMC2 was probed with an anti-LAMC2 antibody. Nuclei were indicated by 4'-6-diamidino-2-phenylindole (*blue*) staining. Scale bar, 43.56 μ m; ITGA6, ITGB4, and CAV1 exhibited increased localization at intracellular compartments in PRA1-knockdown cells compared with the control. Scale bar, 34.82 μ m; TIP47 in PRA1-knockdown cells (K3-2) was increased in intensity at the vesicular compartments. Scale bar, 47.62 μ m.

proteins that are differentially expressed in PRA1-knockdown cells compared with the controls, we conducted two replicates of iTRAQ-based quantitative proteomics analyses (Exp 1 and Exp 2), each of which contained four measurements of two PRA1-knockdown cell clones (K3-2 and K3-14) and two control cell clones (C15 and C15-3), *i.e.* two biologically replicated samples harvested and labeled in parallel (Fig. 3A). The iTRAQ-labeled samples were then analyzed by two-dimensional liquid chromatography-mass spectrometry (LC-MS/MS) for the quantitative proteomic analysis. The two-dimensional fractionation of the labeled peptides involved the use of an offline SCX-based separation in the first dimension, followed by an online reverse phase fractionation. Each fraction was analyzed in two independent mass spectrometer runs. The resulting MS/MS spectra were analyzed using the nonredundant International Protein Index human sequence data-

base (Version 3.27) with the MASCOT algorithm. The search results were further evaluated using the open-source TPP software (version 3.4) with stringent criteria regarding protein probability (≥ 0.95) and at least two peptide hits for one protein identification. The false discovery rate of protein detection was empirically determined by searching the dataset against a random International Protein Index Human database (version 3.27) using the same search parameters and TPP cutoffs. The estimated false discovery rate of 1.1% was calculated as the number of reverse proteins divided by the number of forward proteins.

Using this approach, we identified 1137 nonredundant proteins and quantified 1119 of them in Exp 1 (Fig. 3B; [Supplementary Table S1](#)). A comparable number of proteins were identified (1119) and quantified (1047) in Exp 2 (Fig. 3B; [Supplementary Table S2](#)). Among the quantified proteins, 861

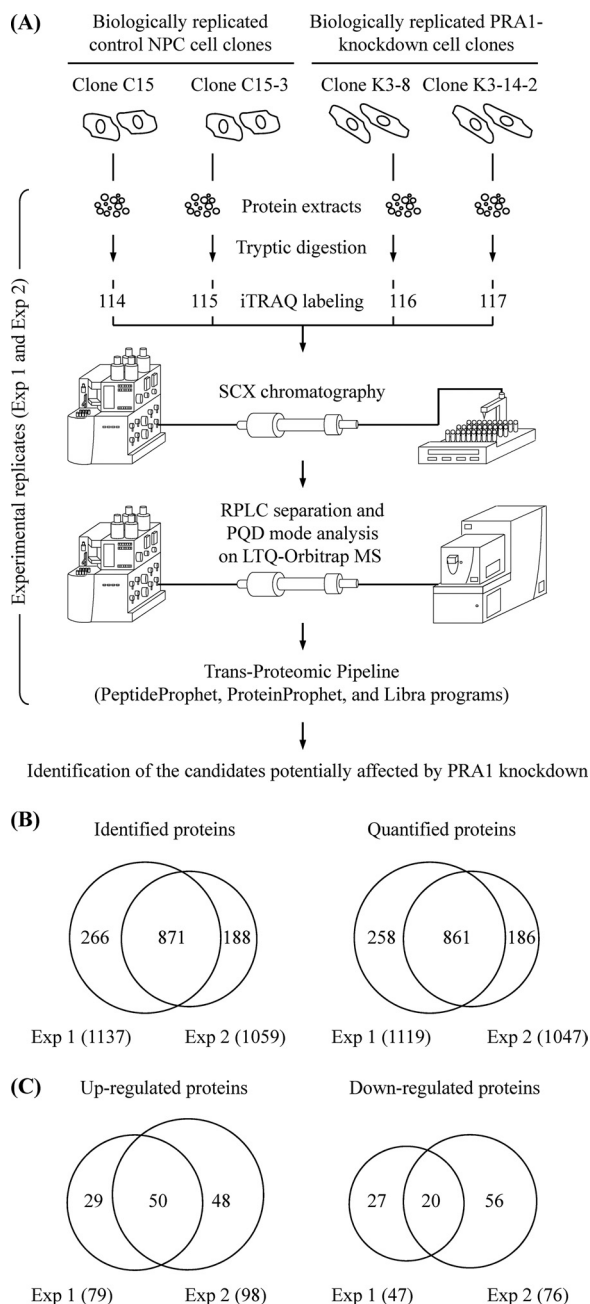


FIG. 3. Identification of differentially expressed proteins in PRA1-knockdown NPC cell clones. A, Schematic diagram showing the workflow designed for profiling of the PRA1-affected proteins by iTRAQ-based analysis. The cell extracts were individually harvested from two control NPC cell clones and two PRA1-knockdown cell clones. These protein extracts were trypsin-digested, and the resulting peptides from each of four samples were labeled with corresponding iTRAQ reporters in parallel. The iTRAQ-labeled peptides were then pooled and applied to strong cation exchange (SCX) chromatography for fractionation, followed by reverse-phase liquid chromatography (RPLC) for further separation. The peptide identities and intensities were analyzed by LTQ-Orbitrap MS with PQD mode. Data analyses were then performed with the PeptideProphet, ProteinProphet, and Libra programs in the Trans-Proteomic Pipeline using the MASCOT algorithm as the search engine. As indicated, the iTRAQ

proteins existed both in Exp 1 and Exp 2 (Fig. 3B). Because each of tested samples was derived from an independent cell clone, each of the knockdown data was then ratioed to both controls to minimize the possibility that the proteome-wide changes actually resulted from a selective effect of individual cell clone, rather than from PRA1 depletion. Based on this, each of the reported proteins was attributed with four sets [K3-8/C15 (116/114); K3-8/C15-3 (116/115); K3-14/C15 (117/114); K3-14/C15-3 (117/115)] of iTRAQ ratios in each experiment (Supplementary Tables S1 and S2). Only the proteins differentially displayed in at least two sets were considered as potential candidates that were differentially expressed in PRA1-knockdown cells. This approach ensures the probability for identification of candidates potentially affected by PRA1 knockdown irrespective of the cell clone background. The considerable candidates included 126 and 174 differentially expressed proteins, identified in Exp 1 and Exp 2, respectively (Fig 3C; Supplementary Tables S3 and S4). Among them, 50 proteins with higher expression levels and 20 proteins with lower expression levels in the knockdown cells were consistently shown in two experimental replicates (Fig 3C; Table I).

Selection of Candidates Potentially Affected by PRA1 Knockdown—Ontological analysis of these 70 proteins highlighted that eight and nine of the proteins reportedly contribute to lipid metabolism/transport and cell adhesion and migration, respectively (Table II). Biological network analysis using MetaCore software further deduced the functional connections among these proteins (Supplementary Table S5), especially associated with organic acid transport and cell adhesion processes (Supplementary Fig. S2). These biological processes are related to cancer development, and also are relevant to PRA1-associated cell morphology changes (Fig. 1). In the list, laminin subunit γ -2 (LAMC2) has been reported to be over-expressed by tumor cells of the invasive front or tumor-stroma interface of many carcinomas (34, 35). LAMC2 composes a major component of epithelial basement membrane, laminin-5. ITGA6 and ITGB4 can form a heterodimer (α 6 β 4 integrin), which functions as a receptor for laminin-5. Both ITGA6 and ITGB4 have been shown to act in promoting carcinoma migration (36–38).

The tail-interacting protein of 47 kDa (TIP47), alternatively named as mannose-6-phosphate receptor-binding protein 1 (MPRBP1) or perilipin 3, is a Rab9 effector protein, which binds both to Rab9 and to the mannose 6-phosphate

experiment was conducted in duplicate (shown as Exp 1 and Exp 2). B, Number of proteins identified or quantified in two iTRAQ-based experiments. Venn diagrams show overlap between proteins identified or quantified in the two experiments. The total number of proteins identified or quantified in each experiment is listed in brackets. C, Number of proteins identified to be up-regulated or down-regulated in two iTRAQ-based experiments. Venn diagrams show overlap between proteins up-regulated or down-regulated in the two experiments. The total number of proteins up-regulated or down-regulated in each experiment is listed in brackets.

TABLE I
List of differentially expressed proteins in PRA1-knockdown NPC cell clones identified both in Exp 1 and Exp 2

Accession No.	Protein name (Gene name)	Experiment	ProteinProphet probability ^a	No. of identified peptides	Percent coverage (%)	ITRAQ ratios (mean ± S.D.) ^b			No. of spectra for quantification	No. of unique peptides for quantification	GO biological process category ^d	
						K3-8/C15 ^c (116/114)	K3-14/C15 ^c (117/114)	K3-14/C15-3 ^c (117/115)				
Up-regulated proteins												
IP100005102.3	Spermine synthase (SMS)	1	1.00	4	14.5	1.18 ± 0.24	1.06 ± 0.16	1.50 ± 0.26	14	4	spermine biosynthetic process	
IP100007797.3	Fatty acid-binding protein, epidermal (FABP5)	2	1.00	5	10.4	1.19 ± 0.26	0.99 ± 0.20	1.54 ± 0.19	12	3	lipid metabolic process; epidermis development	
IP100008475.1	Hydroxymethylglutaryl-CoA synthase, cytoplasmic (HMGCS1)	1	1.00	4	28.1	1.25 ± 0.24	1.57 ± 0.44	1.47 ± 0.34	15	4	cholesterol biosynthetic process	
IP100008986.1	Large neutral amino acids transporter small subunit 1 (SLC7A5)	2	1.00	3	8.3	1.32 ± 0.30	1.58 ± 0.36	1.48 ± 0.26	11	4	amino acid transport	
IP100009236.5	Isoform Alpha of Caveolin-1 (CAV1)	2	1.00	2	7.3	1.57 ± 0.46	1.09 ± 0.08	1.55 ± 0.51	22	2	cholesterol homeostasis; cholesterol transport; endocytosis	
IP100009943.2	Tumor protein, translationally-controlled 1 (TPT1)	1	1.00	2	16.9	1.62 ± 0.44	1.68 ± 0.45	2.26 ± 0.47	2.35 ± 0.50	14	2	—
IP100010214.1	Protein S100-A14 (S100A14)	1	1.00	5	35.6	1.03 ± 0.21	1.45 ± 0.40	1.39 ± 0.26	1.99 ± 0.59	35	5	calcium ion binding; chemokine receptor binding
IP100010471.5	Plastin-2 (LCP1)	2	1.00	3	27.9	1.02 ± 0.30	1.23 ± 0.32	1.31 ± 0.38	1.57 ± 0.40	28	2	regulation of intracellular protein transport
IP100010697.1	Isoform Alpha-6X1X2B of Integrin alpha-6 precursor (ITGA6)	1	1.00	20	52.6	1.06 ± 0.23	0.91 ± 0.12	1.60 ± 0.40	1.37 ± 0.21	157	19	cell adhesion; integrin-mediated signaling pathway
IP100010860.1	Isoform p27-L of 26S proteasome non-ATPase regulatory subunit 9 (PSMD9)	2	1.00	2	22.0	1.43 ± 0.31	1.45 ± 0.20	0.95 ± 0.21	0.97 ± 0.13	12	2	proteasomal ubiquitin-dependent protein catabolic process
IP100011266.6	26S protease regulatory subunit 4 (PSMC1)	2	1.00	8	35.2	1.33 ± 0.40	1.03 ± 0.23	1.38 ± 0.50	1.05 ± 0.19	41	7	proteasomal ubiquitin-dependent protein catabolic process
IP100011200.5	D-3-phosphoglycerate dehydrogenase (PHGDH)	2	1.00	9	32.0	1.50 ± 0.64	0.87 ± 0.20	1.91 ± 1.23	1.00 ± 0.16	26	6	amino-acid biosynthesis
IP100011250.3	Ubiquitin carboxyl-terminal hydrolase isozyme L3 (UCHL3)	1	1.00	8	25.7	1.54 ± 0.41	1.05 ± 0.11	1.38 ± 0.39	0.94 ± 0.09	71	8	ubiquitin-dependent protein catabolic process
IP100013890.2	Isoform 1 of 14-3-3 protein sigma (SFN)	2	1.00	7	21.0	1.44 ± 0.38	0.98 ± 0.12	1.34 ± 0.34	0.91 ± 0.09	66	6	DNA damage response
IP100014197.2	Protein CDV3 homolog (CDV3)	2	1.00	5	46.1	1.06 ± 0.16	1.28 ± 0.29	1.42 ± 0.24	1.74 ± 0.52	25	4	cell proliferation
IP100015117.2	Isoform Long of Laminin subunit gamma-2 precursor (LAMC2)	1	0.99	6	35.7	1.14 ± 0.39	1.21 ± 0.46	1.46 ± 0.53	1.55 ± 0.60	21	5	cell adhesion; epidermis development
IP100016832.1	Isoform Short of Proteasome subunit alpha type 1 (PSMA1)	2	1.00	9	48.3	1.70 ± 1.37	1.12 ± 0.25	1.34 ± 0.90	0.94 ± 0.17	42	7	proteasomal ubiquitin-dependent protein catabolic process
IP100017448.1	40S ribosomal protein S21 (RPS21)	2	1.00	10	27.0	1.85 ± 1.35	1.05 ± 0.20	1.53 ± 0.92	0.93 ± 0.19	30	4	translational elongation
IP100017450.2	Transcription initiation factor IIF subunit alpha (GTF2F1)	2	1.00	4	54.2	1.66 ± 0.48	0.98 ± 0.09	1.58 ± 0.48	0.93 ± 0.08	28	4	transcription regulation
IP100017704.3	Coactosin-like protein (COTL1)	2	1.00	3	7.4	1.26 ± 0.35	0.81 ± 0.12	1.42 ± 0.40	0.91 ± 0.08	10	3	actin binding; enzyme binding
IP100018219.1	Transforming growth factor-beta-induced protein ig-h3 precursor (TGFB1)	1	1.00	4	50.5	1.57 ± 0.82	1.06 ± 0.20	1.42 ± 0.61	1.00 ± 0.13	10	3	cell adhesion; negative regulation of cell adhesion
IP100022078.3	Protein NDRG1 (NDRG1)	2	1.00	3	3.8	0.93 ± 0.10	1.13 ± 0.21	1.77 ± 0.33	2.14 ± 0.43	9	2	response to metal ion
IP100024095.3	Annexin A3 (ANXA3)	1	1.00	5	20.3	0.87 ± 0.15	1.48 ± 0.20	1.78 ± 0.35	2.88 ± 0.61	10	2	cell motion; signal transduction
IP100026087.1	Barrier-to-autointegration factor (BANF1)	2	1.00	6	29.4	1.14 ± 0.16	1.02 ± 0.17	1.79 ± 0.26	1.60 ± 0.20	34	3	host-virus interaction
IP100026202.1	60S ribosomal protein L18a (RPL18A)	2	1.00	3	40.4	1.30 ± 0.26	0.90 ± 0.10	1.44 ± 0.28	1.01 ± 0.17	4	2	translational elongation
		1	1.00	7	43.8	1.69 ± 1.44	0.91 ± 0.20	1.51 ± 1.26	0.82 ± 0.11	27	7	
		2	1.00	13	34.7	1.63 ± 1.20	0.99 ± 0.23	1.39 ± 1.04	0.94 ± 0.14	34	6	

TABLE 1—continued

Accession No.	Protein name (Gene name)	Experiment	ProteinProphet probability ^a	No. of identified peptides	Percent coverage (%)	ITRAQ ratios (mean ± S.D.) ^b			No. of spectra for quantification	No. of unique peptides for quantification	GO biological process category
						K3-8/C15 ^c (116/114)	K3-9/C15-3 ^c (116/115)	K3-14/C15-3 ^c (117/115)			
IP100026546.1	Platelet-activating factor acetyltransferase IB subunit beta (PAFAH1B2)	1	1.00	3	18.3	1.33 ± 0.26	0.94 ± 0.11	1.29 ± 0.16	20	2	lipid catabolic process
IP100026813.1	Protein farnesyltransferase/geranylgeranyltransferase type I alpha subunit	2	1.00	3	14.8	1.41 ± 0.25	0.86 ± 0.10	1.31 ± 0.13	18	2	protein amino acid farnesylation
IP100027422.1	Isoform Beta-4C of integrin beta-4 precursor (ITGB4)	2	1.00	3	10.8	1.13 ± 0.28	1.33 ± 0.59	1.31 ± 0.21	7	2	cell-matrix adhesion; integrin-mediated signaling pathway
IP100027493.1	4F2 cell-surface antigen heavy chain (SLC3A2)	1	1.00	16	8.6	1.39 ± 0.43	1.42 ± 0.26	1.64 ± 0.46	55	8	calcium ion transport; amino-acid transport
IP100028091.3	Actin-like protein 3 (ACTR3)	2	1.00	24	39.1	1.36 ± 0.52	1.09 ± 0.19	1.31 ± 0.49	139	14	cell motion; actin filament polymerization
IP100032849.2	UPF0384 protein CGI-117 (NOP16)	2	1.00	9	31.1	1.54 ± 0.62	0.96 ± 0.18	1.74 ± 0.70	31	5	—
IP100062120.1	Protein S100-A16 (S100A16)	1	1.00	2	8.4	1.10 ± 0.41	1.01 ± 0.57	1.68 ± 0.40	6	2	calcium ion binding
IP100171856.1	Deoxyhypusine hydroxylase (DOHH)	2	1.00	3	33.0	1.12 ± 0.22	1.22 ± 0.32	1.40 ± 0.32	17	3	oxidation reduction
IP100218918.5	Annexin A1 (ANXA1)	1	1.00	3	29.1	1.09 ± 0.29	1.10 ± 0.34	1.36 ± 0.41	15	1	cell motion; lipid metabolic process; anti-apoptosis
IP100218993.1	Isoform Beta of Heat-shock protein 105 kDa (HSPH1)	2	1.00	18	26.8	1.64 ± 0.37	1.23 ± 0.39	1.33 ± 0.17	222	5	stress response
IP100219219.3	Galectin-1 (LGALS1)	2	1.00	34	46.4	1.25 ± 0.28	1.24 ± 0.29	1.55 ± 0.37	159	18	regulation of apoptosis
IP100219468.4	Isoform Ila of Profilin-2 (PFN2)	1	1.00	6	51.1	0.85 ± 0.14	0.97 ± 0.16	1.36 ± 0.26	39	6	actin cytoskeleton organization
IP100219953.5	Cytidylylase kinase (CMPK1)	2	1.00	2	20.2	1.40 ± 0.35	0.86 ± 0.13	1.54 ± 0.41	21	1	pyrimidine biosynthesis
IP100220487.4	Isoform 1 of ATP synthase D chain, mitochondrial (ATP5H)	1	1.00	3	12.3	1.62 ± 0.19	0.83 ± 0.09	1.88 ± 0.23	16	2	ATP synthase coupled proton transport
IP1003030300.3	FK506-binding protein 10 precursor (FKBP10)	1	1.00	2	24.2	1.25 ± 0.24	1.25 ± 0.30	1.71 ± 0.73	5	2	protein folding
IP100303882.2	Isoform B of Mannose-6-phosphate receptor-binding protein 1 (TIP47, PLIN3)	2	1.00	4	4.5	0.87 ± 0.17	1.11 ± 0.23	1.71 ± 0.28	8	2	vesicle-mediated transport
IP100306369.3	NOL1/NOP2/Sun domain family 2 protein (NSUN2)	1	1.00	13	30.6	1.11 ± 0.31	0.99 ± 0.12	1.69 ± 0.63	33	6	rRNA methylation
IP100306960.3	Asparaginyl-tRNA synthetase, cytoplasmic (MARS)	2	1.00	3	7.1	1.71 ± 0.65	0.89 ± 0.11	1.44 ± 0.42	8	3	protein biosynthesis
IP100329629.6	DnaJ homolog subfamily C member 7 (DNAJC7)	2	1.00	3	12.2	1.67 ± 0.31	0.91 ± 0.14	1.50 ± 0.40	10	3	protein folding
IP100329801.12	Annexin A5 (ANXA5)	1	1.00	15	57.2	0.92 ± 0.22	0.95 ± 0.17	1.56 ± 0.46	115	15	anti-apoptosis; blood coagulation
IP100465184.3	Guanine deaminase (GDA)	2	1.00	25	52.8	0.92 ± 0.26	0.87 ± 0.18	1.57 ± 0.43	113	14	nucleic acid metabolic process
IP100465260.3	Trifunctional purine biosynthetic protein adenosine-3 (GART)	2	1.00	4	9.1	1.00 ± 0.15	1.31 ± 0.23	1.12 ± 0.24	14	4	purine biosynthesis
IP100470525.5	Glycogen phosphorylase, liver form (PYGL)	1	1.00	8	14.8	1.16 ± 0.22	1.29 ± 0.33	1.30 ± 0.34	19	7	glucose homeostasis; glycogen metabolic process
IP100472082.2	Isoform 1 of Serpin B5 (SERPINB5)	2	1.00	9	15.5	1.24 ± 0.24	1.22 ± 0.23	1.41 ± 0.19	12	5	protein binding
IP100554786.4	Thioredoxin reductase 1, cytoplasmic precursor (TXNRD1)	2	1.00	9	25.7	1.04 ± 0.12	1.13 ± 0.16	1.38 ± 0.27	32	5	cell redox homeostasis; electron transport
Down-regulated proteins											
IP100000873.3	VaiY-HRNA synthetase (VARS)	1	1.00	5	6.2	0.92 ± 0.33	0.68 ± 0.14	0.80 ± 0.17	7	4	translational elongation
IP100011913.1	Heterogeneous nuclear ribonucleoprotein A0 (HNRNPA0)	2	1.00	4	19.0	0.79 ± 0.08	0.71 ± 0.09	0.70 ± 0.10	22	2	mRNA processing

TABLE 1—continued

Accession No.	Protein name (Gene name)	Experiment	ProteinProphet probability ^a	No. of identified peptides	Percent coverage (%)	ITRAQ ratios (mean ± S.D.) ^b			No. of spectra for quantification	No. of unique peptides for quantification	GO biological process category ^d
						K3-8/C15 ^c (116/114)	K3-8/C15-3 ^c (116/115)	K3-14/C15-3 ^c (117/115)			
IP100013495.1	Isoform 2 of ATP-binding cassette sub-family F member 1 (ABCF1)	1	1.00	3	8.9	0.84 ± 0.13	0.81 ± 0.16	0.66 ± 0.12	7	3	inflammatory response; translation
IP100013808.1	Alpha-actinin-4 (ACTN4)	2	1.00	4	5.1	0.85 ± 0.07	0.73 ± 0.10	0.74 ± 0.15	11	3	protein transport; regulation of apoptosis
IP100013871.1	Ribonucleoside-diphosphate reductase large subunit (RRM1)	1	1.00	6	20.0	0.98 ± 0.16	0.69 ± 0.12	0.68 ± 0.13	24	5	DNA replication; oxidation reduction
IP100015688.1	Glypican-1 precursor (GPC1)	2	1.00	5	18.9	0.93 ± 0.15	0.58 ± 0.11	1.02 ± 0.15	14	4	heparan sulfate proteoglycan binding
IP100018452.1	Copine-1 (CPNE1)	1	1.00	2	24.4	0.79 ± 0.16	0.73 ± 0.11	0.70 ± 0.25	15	5	lipid metabolic process; vesicle-mediated transport
IP100018783.1	Inosine triphosphate pyrophosphatase (ITPA)	2	1.00	2	6.6	0.93 ± 0.11	0.76 ± 0.26	0.78 ± 0.19	5	1	nucleotide metabolic process
IP100021700.3	Proliferating cell nuclear antigen (PCNA)	1	1.00	2	9.3	1.02 ± 0.13	0.77 ± 0.12	0.95 ± 0.15	2	2	DNA replication
IP100022977.1	Creatine kinase B-type (CKB)	2	1.00	6	15.8	0.81 ± 0.10	0.53 ± 0.10	1.06 ± 0.12	34	4	creatine metabolic process
IP100031420.3	UDP-glucose 6-dehydrogenase (UGDH)	1	1.00	2	11.7	0.83 ± 0.15	0.50 ± 0.16	1.10 ± 0.15	43	5	DNA replication
IP100032313.1	Protein S100-A4 (S100A4)	2	1.00	2	19.1	0.72 ± 0.13	0.58 ± 0.11	0.96 ± 0.24	5	2	cellular response to stress
IP100033130.3	SUMO-activating enzyme subunit 1 (SAE1)	2	1.00	8	38.3	0.74 ± 0.09	0.62 ± 0.08	0.68 ± 0.08	57	2	ubiquitin-protein ligase activity
IP100034319.2	Isoform A of Protein CutA precursor (CUTA)	1	1.00	13	46.0	0.77 ± 0.12	0.59 ± 0.10	0.73 ± 0.12	54	6	protein localization; response to metal ion
IP100220107.1	Isoform 1 of Transcriptional regulator ATRX (ATRX)	2	1.00	6	34.9	0.90 ± 0.17	0.57 ± 0.10	0.54 ± 0.14	20	4	DNA methylation
IP100293434.2	Signal recognition particle 14 kDa protein (SRP14)	1	1.00	10	35.2	0.96 ± 0.26	0.68 ± 0.26	0.79 ± 0.36	17	5	SRP-dependent cotranslational protein targeting to membrane
IP100375631.6	Interferon-induced 17 kDa protein precursor (ISG15)	2	1.00	4	10.1	0.80 ± 0.13	0.66 ± 0.12	0.74 ± 0.11	9	4	ISG15-protein conjugation
IP100449049.5	Poly [ADP-ribose] polymerase 1 (PARP1)	1	1.00	6	13.2	0.84 ± 0.11	0.70 ± 0.08	0.83 ± 0.09	13	5	DNA repair
IP100644020.1	Sterol O-acyltransferase (Acyl-Coenzyme A: cholesterol acyltransferase) 1 (SOAT1)	2	1.00	2	18.8	1.11 ± 0.13	1.25 ± 0.11	0.23 ± 0.05	19	2	cholesterol metabolic process
IP100646304.4	Peptidylprolyl isomerase B precursor (PPIB)	1	1.00	3	12.7	0.75 ± 0.11	1.12 ± 0.16	0.32 ± 0.09	33	2	protein folding

^a Protein probability obtained from the ProteinProphet software.

^b Mean, a weighted average of the peptide ratios per protein; S.D., standard deviation calculated among the peptide ratios per protein.

^c C15 and C15-3, two independent mock clones; K3-8 and K3-14, two independent PRA1-knockdown stable clones.

^d Functional classification of the dysregulated proteins as revealed by annotation in the GO biological process categories.

TABLE II
List of selected candidates potentially affected by PRA1 knockdown

Accession No.	Protein name	Gene name	GO biological process category ^a	Protein level in PRA1-knockdown cells
Lipid transport/metabolism-related				
IP100007797.3	Fatty acid-binding protein, epidermal	FABP5	lipid metabolic process; epidermis development	up-regulation
IP100008475.1	Hydroxymethylglutaryl-CoA synthase, cytoplasmic	HMGCS1	cholesterol biosynthetic process	up-regulation
IP100009236.5	Isoform Alpha of Caveolin-1	CAV1	cholesterol homeostasis; cholesterol transport; endocytosis	up-regulation
IP100018452.1	Copine-1	CPNE1	lipid metabolic process; vesicle-mediated transport	down-regulation
IP100026546.1	Platelet-activating factor acetylhydrolase IB subunit beta	PAFAH1B2	lipid catabolic process	up-regulation
IP100218918.5	Annexin A1	ANXA1	cell motion; lipid metabolic process; anti-apoptosis	up-regulation
IP100303882.2	Isoform B of Mannose-6-phosphate receptor-binding protein 1	TIP47	vesicle-mediated transport	up-regulation
IP100644020.1	Sterol O-acyltransferase (Acyl-Coenzyme A: cholesterol acyltransferase) 1	SOAT1	cholesterol metabolic process	down-regulation
Cell adhesion/migration-related				
IP100010697.1	Isoform Alpha-6X1X2B of Integrin alpha-6 precursor	ITGA6	cell adhesion; integrin-mediated signaling pathway	up-regulation
IP100015117.2	Isoform Long of Laminin subunit gamma-2 precursor	LAMC2	cell adhesion; epidermis development	up-regulation
IP100027422.1	Isoform Beta-4C of Integrin beta-4 precursor	ITGB4	cell-matrix adhesion; integrin-mediated signaling pathway	up-regulation
IP100018219.1	Transforming growth factor-beta-induced protein ig-h3 precursor	TGFB1	cell adhesion; negative regulation of cell adhesion	up-regulation
IP100024095.3	Annexin A3	ANXA3	cell motion; signal transduction	up-regulation
IP100028091.3	Actin-like protein 3	ACTR3	cell motion; actin filament polymerization	up-regulation
IP100218918.5	Annexin A1	ANXA1	cell motion; lipid metabolic process; anti-apoptosis	up-regulation
IP100219468.4	Isoform Ila of Profilin-2	PFN2	actin cytoskeleton organization	up-regulation
IP100032313.1	Protein S100-A4	S100A4	epithelial to mesenchymal transition	down-regulation

^a Functional classification of the dysregulated proteins as revealed by annotation in the GO biological process categories.

receptors (MPRs) (Supplementary Fig. S2A). TIP47 is required for MPRs recycling from late endosomes to the Golgi complex (39–41); importantly, this pathway also contributes to lipid (such as cholesterol) export (42, 43). In addition, the epidermal fatty acid-binding protein (FABP5) is postulated to serve as a lipid shuttle; an elevation of FABP5 may be necessary for the activation of cell motility within regenerative epidermis during wound healing (44). It is also notable that caveolin-1 (CAV1), the primary structural component of caveolae, is implicated in the processes of vesicular transport, cholesterol balance, transformation, and tumorigenesis (45, 46). Considering these facts, we sought to validate the expression of selected candidates, including the above, in PRA1-knockdown cells and to further explore their roles in PRA1-involved functions.

Validation of Proteins Differentially Expressed in PRA1-knockdown Cells—We first performed Western blot analysis to validate the protein levels of selected candidates in PRA1-knockdown cells. To truly reflect the effect of PRA1 knockdown, we prepared the cell extracts from other cell clones, and extended the number of tested cell clones (four knockdown clones, three control clones, and the parental cells) in the validation experiments to exclude biological variations among cell clones. As shown in Fig. 2A, each of the selected proteins, including LAMC2, ITGA6, ITGB4, FABP5, CAV1, TIP47, PFN2, and annexin A3, showed elevated protein levels, albeit at varied magnitudes, in four PRA1-knockdown clones (K3–2, K3–14, K3–8, and K3–7) compared with three control clones (C13, C15, and C15–3) and the parental NPC-TW04 cells. These results confirmed the trend reported by the iTRAQ experiments (Table I), which implicated the elevated levels of these proteins in PRA1-knockdown cells. Using quantitative RT-PCR analysis, we further examined whether the mRNA levels of these proteins were elevated in parallel with their protein levels in PRA1-knockdown clones. As shown in Supplementary Fig. S1B, the mRNA levels of LAMC2, ITGA6, ITGB4, FABP5, CAV1, and TIP47 were increased in average to 4.7, 1.4, 2.7, 3.5, 2.5, and 1.5 fold, respectively, in three PRA1-knockdown clones. The data suggested that the above proteins were increased both at transcriptional and post-transcriptional levels in PRA1-knockdown cells.

Altered Localization of the Affected Proteins in PRA1-knockdown Cells—To evaluate the cellular localization of the proteins affected by PRA1 knockdown, we selectively performed immunofluorescent staining of LAMC2, ITGA6, ITGB4, CAV1, and TIP47 in PRA1-knockdown cells. As shown in Fig. 2B (also in Supplementary Fig. S3), the overall staining intensities of these proteins were increased in PRA1-knockdown cells, correlating with their elevated protein levels revealed by Western blotting (Fig. 2A). In addition, the perinuclear pools of ITGA6, ITGB4, and CAV1 were apparently increased in PRA1-knockdown cells, indicating that PRA1 depletion also resulted in spatial alteration of these proteins.

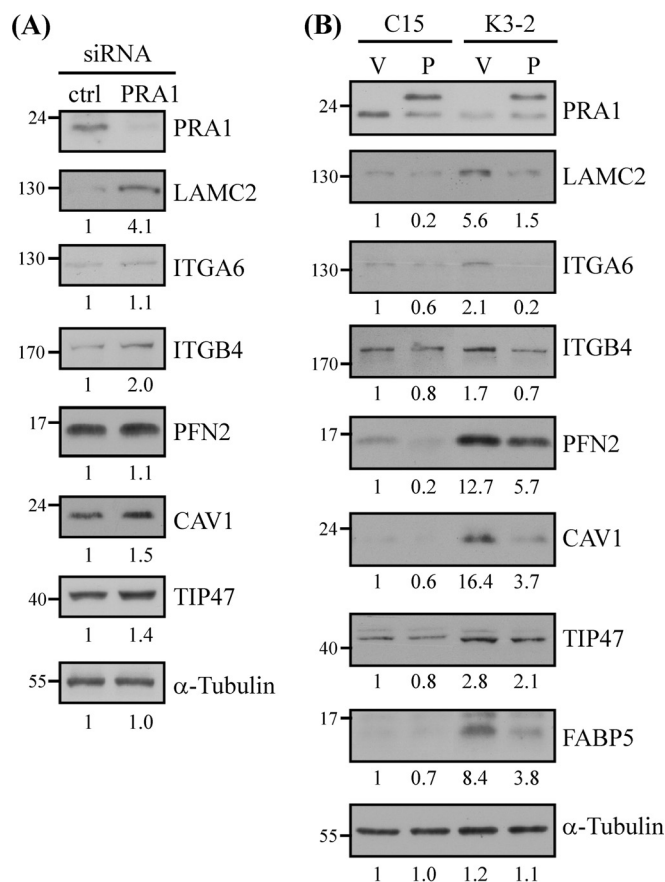


Fig. 4. Association of PRA1 with the expression levels of the affected proteins. A, Effect of transient knockdown of PRA1 on the levels of affected proteins. Protein extracts were individually harvested from NPC-TW04 cells, which had been transfected with PRA1 siRNA or scramble control siRNA for 72 h. The extracts were then analyzed by Western blot using antibodies as indicated. Numbers represent relative fold differences of protein levels on the basis of densitometer quantitation. B, Re-expression of PRA1 in PRA1-knockdown cells. PRA1-knockdown cells (K3–2) and control cells (C15–3) were pretransfected with plasmids encoding vehicle alone (denoted as V) or HA-tagged PRA1m (denoted as P), which is irresponsive to PRA1-siRNA interference. Protein lysates were harvested 48 h later and applied to Western blot analysis. Numbers represent relative fold differences of protein levels as previously described.

Association of PRA1 with the Expression Levels of the Affected Proteins—To further confirm the effect of PRA1 knockdown on the levels of the affected proteins, we used an alternative siRNA-based approach. We examined the expression levels of selected proteins in NPC cells, which had been transfected with PRA1 siRNA duplex for 72 h. As shown in Fig. 4A, siRNA-mediated depletion of PRA1 caused elevated protein levels of LAMC2 (4.1-fold), ITGB4 (2-fold), CAV1 (1.5-fold), and TIP47 (1.4-fold) as compared with the control-siRNA transfectants, indicating that transient knockdown of PRA1 led to dysregulation of the above proteins.

To reinforce the effect of PRA1, we next examined whether reintroduction of PRA1 into its knockdown cell clones was able to restore PRA1 function in relation to the protein levels

of the affected proteins. As shown in Fig. 4B, ectopically expressed PRA1 in the knockdown cells was able to alleviate the dysregulated expression of LAMC2, ITGA6, ITGB4, CAV1, FABP5, TIP47 and PFN2. Notably, ectopically expressed PRA1 also reduced the expression levels of the above proteins in the control cells. The data collectively demonstrated a role of PRA1 in regulating the expression levels of these PRA1-affected proteins. Based on the fact that PRA1 has not been characterized as a regulator of protein expression levels, the results implicate that dysregulated expression of the affected proteins likely arose as a consequence of biological process impairment by PRA1 knockdown.

The Cholesterol Transport Inhibitor, U18666A, Phenocopied the Effect of PRA1 Knockdown—The results that PRA1 affected the expression levels of CAV1, FABP5, and TIP47, which were involved in cellular lipid homeostasis, prompted us to evaluate whether PRA1 knockdown affected cellular cholesterol distribution. Using filipin labeling of cellular cholesterol, we visualized the distribution of cellular cholesterol in PRA1-knockdown cells. As shown in Fig. 5A (also in [Supplementary Fig. S4A](#)), we observed the intracellular accumulation of cholesterol at vesicular compartments in the knockdown cells (K3-2) compared with the control cells (C15-3). Treating NPC-TW04 cells with U18666A, a reagent known to inhibit cellular cholesterol efflux (47, 48), was used as a positive control (Fig. 5A, *bottom panels*), which morphologically resembled the phenotype of PRA1-knockdown cells. The data revealed that PRA1 depletion affected the process of cholesterol transport.

To further evaluate whether the levels of the proteins affected by PRA1 depletion associated with impaired cholesterol transport, we conducted Western blotting to analyze the protein levels of affected proteins in U18666A-treated NPC cells. As shown in Fig. 5B, the protein levels of LAMC2, ITGA6, ITGB4, CAV1, and TIP47 were respectively increased to 1.6, 1.6, 1.8, 1.3, and 1.6 fold under U18666A treatment, revealing that excessive cholesterol accumulation affected the protein levels of these proteins. Notably, the expression level of PRA1 itself was also 2.5-fold increased in the same situation, indicating that PRA1 responded to impaired cholesterol homeostasis *via* increasing its expression level.

Through overexpression of PRA1 in U18666A-treated cells, we intended to better elucidate the role of PRA1 in regulating the levels of the affected proteins in response to altered cholesterol homeostasis. The results showed that ectopically expressed PRA1 was able to alleviate the U18666A-induced dysregulation of the above proteins (Fig. 5B). Altogether, the data demonstrated that PRA1 knockdown led to impaired cellular cholesterol efflux, resulting in elevated expression levels of the PRA1-affected proteins that were involved in lipid transport and cell migration.

Elevated Levels of PRA1-affected Proteins in LMP1-expressing Cells, Which Showed Functional Interference of PRA1—We have demonstrated that PRA1 is critical for the trafficking and signaling of LMP1 (16). However, it is not clear

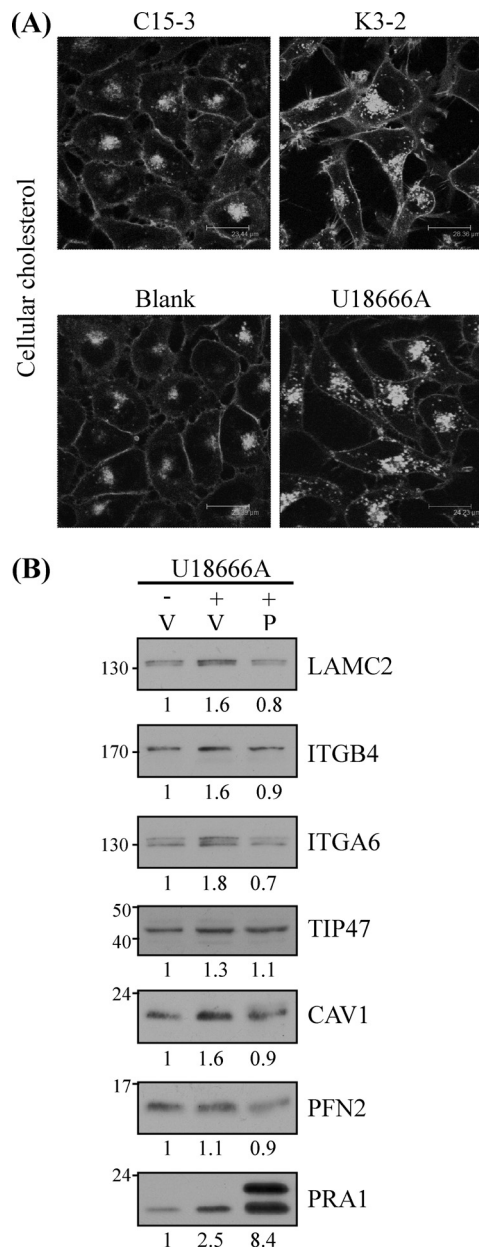


FIG. 5. U18666A treatment phenocopied the effect of PRA1 knockdown in NPC cells. A, Cellular cholesterol accumulation in PRA1-knockdown cells. Cellular cholesterol in PRA1-knockdown (K3-2) or control (C15-3) cells were visualized by filipin staining as detailed under “Experimental Procedures.” NPC-TW04 cells preincubated with 3 μ M U18666A, a hydrophobic amine known to impair cholesterol efflux, were harvested 20 h later for a positive demonstration of cholesterol accumulation. Scale bar, 25–30 μ m. B, Ectopic expression of PRA1 alleviated protein dysregulation by U18666A. NPC-TW04 cells pretransfected with plasmids for HA-tagged PRA1 (denoted as P) or vehicle alone (denoted as V) were incubated with or without 3 μ M U18666A at 24 h post-transfection. After another 20 h, protein lysates from each treatment were harvested and analyzed by Western blot using indicated antibodies. Numbers represent relative fold differences of protein levels.

whether LMP1 interaction with PRA1 will inversely affect the physical function of PRA1, for instance, its intracellular localization. Based on this, we performed subcellular fractionation to analyze PRA1 distribution in LMP1-expressing NPC cells. As shown in Fig. 6A, PRA1 was redistributed to the LMP1-expressing fractions (fractions 7–11), whereas it was more widely distributed in fractions 7–25 in the neo control cells. Moreover, this LMP1-mediated PRA1 redistribution was similarly observed in NPC cells with transient expression of LMP1 but not its truncated form lacking the PRA1-binding domain (LMP1 $_{\Delta TM}$; data not shown), indicating that LMP1 affected the localization of PRA1 likely through interacting with PRA1.

We next investigated the functional consequence of this PRA1 sequestration *via* validating the levels of PRA1-affected proteins in LMP1-expressing cells. We found that the protein levels of LAMC2, ITGA6, ITGB4, CAV1, TIP47, FABP5, and PFN2 were increased in each of two LMP1-expressing cell clones compared with the neo control (Fig. 6B), correlating with the trend reflected in PRA1-knockdown cell clones (Fig. 2A). In addition, these LMP1-expressing cells showed phenotypic changes similar to those shown by PRA1-knockdown cells, including elongated cell shape, increased cell motility, and intracellular cholesterol accumulation (Supplementary Fig. S5A–C).

To better elucidate the role of PRA1 in the LMP1-associated increase of PRA1-affected proteins, we analyzed the levels of selected proteins in NPC cells, which had been transiently transfected with various amounts of expression vectors encoding LMP1 or its truncated form (LMP1 $_{\Delta TM}$) lacking the PRA1-binding domains. Compared with the vector control (without pLMP1 transfection), the protein levels of LAMC2, ITGA6, ITGB4, CAV1, TIP47, and PFN2 were increased in relation to LMP1 expression in NPC-TW04 cells (Fig. 6C). However, the levels of these proteins were unaffected by LMP1 $_{\Delta TM}$ expression regardless of its expression extents (Supplementary Fig. S5D). The data collectively suggested that LMP1 interaction with PRA1 may sequester PRA1 from the sites where it physically functions, thereby affecting the cellular cholesterol distribution and elevating the expression levels of relevant PRA1-affected proteins. These data provided a mechanistic interpretation for LMP1-associated morphogenesis of NPC cells in terms of PRA1.

Elevated Levels of PRA1-affected Proteins in NPC Tissues—To evaluate physiological relevance of the protein dysregulation by PRA1, we performed immunohistochemistry to examine the expression patterns of relevant proteins (CAV1, LAMC2, ITGA6, and ITGB4) together with PRA1 and LMP1 in ten NPC specimens, including three cases with adjacent nontumor epithelia (case numbers 1–3). The staining results were scored as negative, weak, moderate, or strong expression (details under “Experimental Procedures”). NPC tissues, where LMP1 is positive, showed higher expression of CAV1, LAMC2, ITGA6, and ITGB4, in contrast to the nontumor counterparts without LMP1 expression (Fig. 7A). The representa-

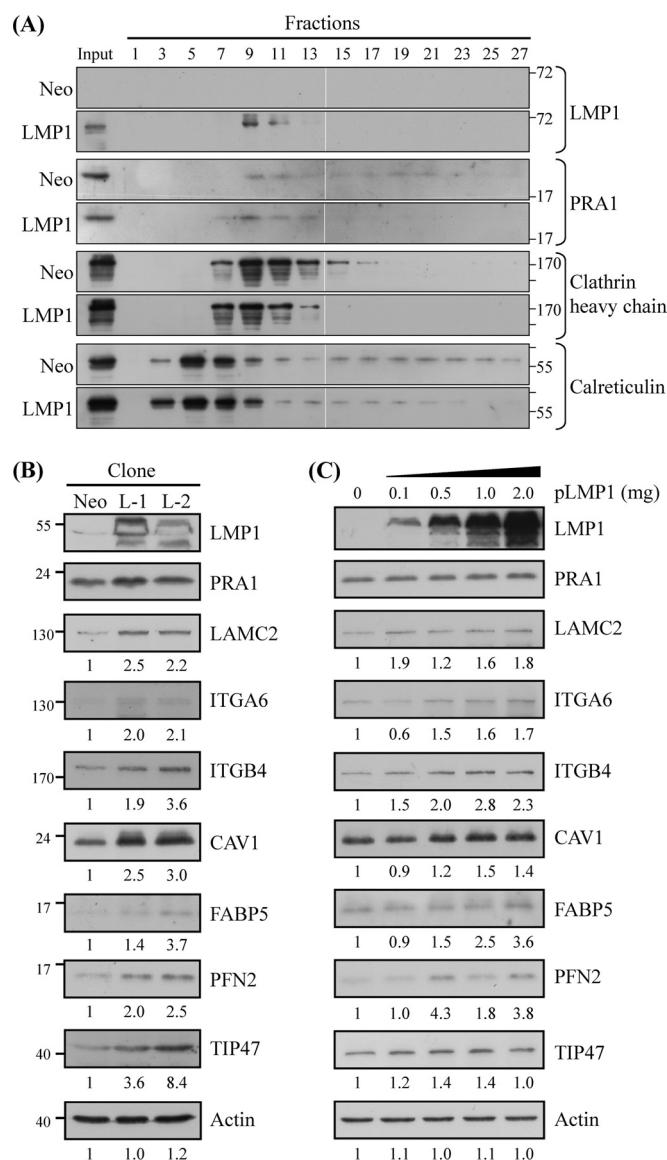


FIG. 6. Elevated levels of PRA1-affected proteins in LMP1-expressing cells, which showed PRA1 sequestration. *A*, Sequestration of PRA1 in LMP1-expressing NPC cell clones. Cell extracts from NPC cells which persistently expressed LMP1 (LMP1) or mock control (Neo) were prepared and subjected to subcellular fractionation as described under “Experimental Procedures.” Every other fraction was analyzed by Western blotting using the indicated antibodies. Calreticulin and clathrin heavy chain were used as markers for endoplasmic reticulum (ER) and post-Golgi apparatus, respectively. *B*, Elevated expression levels of PRA1-affected proteins in LMP1-expressing cells. Protein lysates were individually extracted from two LMP1 stable clones and the neo control. In *C*, NPC-TW04 cells were transfected with various amounts of plasmids encoding FLAG-tagged LMP1 (pLMP1) and cultured for 24 h. Each of the resulting lysates was applied to Western blot analysis using antibodies as indicated. Actin was used as a loading control. Numbers represent relative fold differences of protein levels.

tive expression patterns for CAV1, LAMC2, ITGA6, and ITGB4 in one case containing nontumor counterparts were present in Fig. 7B. The distribution of PRA1 was changed from predom-

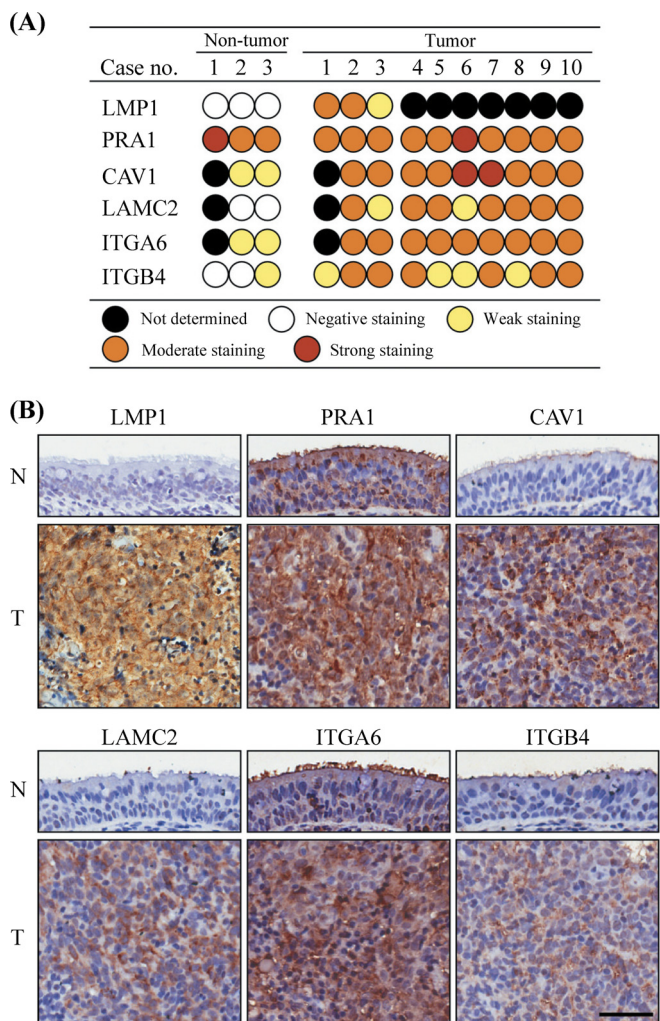


FIG. 7. Elevated levels of PRA1-affected proteins in NPC tissues. A, IHC staining scores for the selected proteins in 10 NPC tissue specimens, including three cases with adjacent nontumor epithelia (case numbers 1–3). Consecutive NPC tissue sections were immunohistochemically stained for these proteins and scored as described under “Experimental Procedures.” B, Representative IHC patterns for the selected proteins in NPC tissues versus the adjacent nontumor counterparts. Original magnification, 400×. Scale bar, 100 μm.

inant localization at the intracellular compartments in adjacent nontumor epithelial cells, to a dispersed pattern in NPC tissues co-expressing LMP1 (*upper-left panels*). Coincidentally, the intracellular portions of CAV1, LAMC2, ITGA6, and ITGB4 were increased in NPC tissues compared with the nontumor counterparts (*upper-right and lower panels*), providing a relevance to the results revealed in NPC cell lines.

To reinforce the significance, we further consulted the Human Protein Atlas, a database containing the immunohistochemical staining profiles of numerous proteins in a variety of cancerous and noncancerous tissues (49, 50), for analyzing the expression profiles of selected PRA1-affected proteins in normal nasopharynx versus the head-and-neck cancer, a

cancer type that is most relevant to NPC among accessible cancerous tissues in Human Protein Atlas. As shown in [Supplementary Table S6](#), the expression extents of CAV1, FABP5, LAMC2, ITGB4, and ITGA6 were overall elevated in the head-and-neck cancerous tissues compared with normal nasopharyngeal epithelia, indicating a favorable correlation between the above proteins and cancers.

DISCUSSION

PRA1 is potentially implicated in numerous cellular processes, whereas lots of its functions still remain to be clarified. Using iTRAQ-based quantitative proteomics analysis, we demonstrated for the first time that inhibition of expression or function of PRA1 led to global changes in the levels of cellular proteins. Among them, a panel of proteins is found to be functionally linked with the networks regulating cellular lipid homeostasis and cell migration, which are related to cancer development. Based on this, our study advances the understanding of the functional properties of PRA1 and their correlation with human diseases.

The ratios of affected proteins revealed by iTRAQ quantification in this study are statistically meaningful and can be validated by Western blot analysis (Fig. 4), although they seem less impressive at their magnitudes. Technically, although iTRAQ possesses the potential to provide accurate quantification spanning two orders of magnitudes, it is limited by (i) isotopic impurities, a manufacturing issue, and (ii) peptide cofragmentation, a problem of sample complexity (51), implying that the reagents tend to “underestimate” the abundance of protein in certain cases. In a properly designed experiment, users can safely rely on iTRAQ-reported trend, but not their magnitudes; for that, validation and follow-up experiments using orthogonal methods are necessary (51). In agreement, we first extended the tested sample sizes in validation experiments (Fig 2A). We then conducted an alternative experiment using a siRNA-based approach to confirm the effect of PRA1 knockdown on relevant protein expression (Fig 4A). We further conducted the experiments reintroducing PRA1 expression in knock-down cells to restore its function in relation to relevant protein expression (Fig. 4B). Finally, we validated the increased levels of the relevant proteins in cells, which showed functional interference of PRA1 (Fig. 6). Altogether, we used combinatorial approaches to clearly demonstrate that PRA1 indeed affected protein levels of selected proteins initially revealed by iTRAQ quantification.

Apart from the recognized function of PRA1 in vesicle trafficking, we herein further find out that PRA1 has important roles in modulating lipid transport and cell migration. Expressional or functional block of PRA1 can affect cellular cholesterol efflux in NPC cells and elicit responses to adapt the impairments, rendering NPC cells to change cell shape and motility (Fig. 8A). Cholesterol is an essential structural component in the cell membranes of most vertebrates; it also

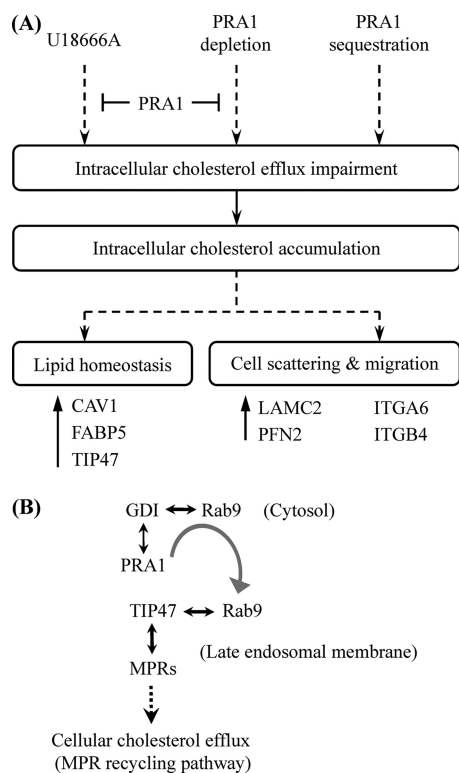


FIG. 8. A, A model depicting the role of PRA1 in morphogenesis of NPC cells. PRA1 knockdown affects cellular cholesterol transport, thereby causing cellular cholesterol accumulation reminiscent of the effect of U18666A. This cholesterol accumulation elicits adaptive responses, leading to elevated expression levels of selected proteins, such as CAV1, FABP5, and TIP47, which modulate lipid homeostasis and transport. This altered lipid homeostasis coincidentally results in increased expression levels of proteins involved in cell scattering and migration (such as LAMC2, ITGA6, and ITGB4), concomitant with altered intracellular localization of these proteins. Moreover, overexpressed PRA1 can alleviate the dysregulation of these proteins by PRA1 depletion or U18666A treatment, indicating that PRA1 can regulate the levels of these proteins in response to altered lipid homeostasis. EBV-encoded LMP1 can sequester PRA1 through interaction with PRA1, leading to a spatially functional interference of PRA1, consistent with the effect of PRA1 depletion. Altogether, this model delineates the PRA1-associated proteome-wide dysregulation in relation to lipid homeostasis and cell migration, implicating a physiological relevance of PRA1-involved functions in LMP1-associated morphogenesis of NPC. **B,** Interplay of PRA1 with Rab9 and TIP47 and the relevance implicated in lipid homeostasis. Rab9 is localized at the late endosomes and involved in the recycling of MPRs. PRA1 dissociates Rab9 from GDI-bound complexes in the cytosol and then escorts the liberated Rab9 to the late-endosomal membranes (9). Once localized to the membranes, Rab9 binds to its effector TIP47, which in turn triggers MPRs recycling from late endosomes to the Golgi complex (39–41). This recycling pathway is also implicated to mediate cholesterol export (42, 43, 52).

modulates the functions of membrane proteins and participates in several membrane trafficking and transmembrane signaling processes (52). The mechanism underlying how PRA1 modulates cholesterol transport awaits in-depth clarification, however, one of the possibilities could be the PRA1-involved regulation of Rab9, a Rab localized at the late endo-

somes and involved in the recycling of MPRs (Fig. 8B). In agreement with this, overexpressed Rab9 is able to relieve the cholesterol accumulation in fibroblasts of Niemann-Pick type C disease, a lipidosis characterized by excessive accumulation of free cholesterol as well as fatty acids in the late endosomal/lysosomal system (53, 54). Based on these facts, PRA1 is likely to regulate the cellular cholesterol egress in terms of Rab9. Our data showed that the expression level of TIP47 was elevated both by U18666A treatment, which is known to resemble the phenotype of Niemann-Pick type C disease (55), and PRA1 depletion (Figs. 2, 4, and 5), functionally linking PRA1 for the first time to the interplay of Rab9 with TIP47. This functional linkage additionally raises the likelihood as proposed in Fig. 8B. Although not being a known cholesterol-binding protein, PRA1 by itself may alternatively act as a cholesterol regulator. This idea is encouraged by the amino acid analysis revealing that PRA1 possesses a cholesterol-binding domain ($_{102}L/V-X_{1-5}-Y-X_{1-5}-K/R_{113}$), as shown in the case of cholesterol-binding protein, σ -1 receptor (56).

In addition to TIP47, PRA1 depletion also affected the expression of LAMC2, ITGA6, ITGB4, CAV1, and FABP5 both at transcriptional and post-transcriptional levels (Fig. 2A; Supplementary Fig. S1B). Owing to a lack of evidence delineating involvement of PRA1 in transcriptional regulation, the dysregulated mRNA expression of the above proteins may arise, at least in part, from cholesterol accumulation by PRA1 depletion. In agreement with this, the expression levels of these proteins were elevated in response to U18666A treatment and can be alleviated by over-expressed PRA1 (Fig. 5B). Notably, the protein expression of endogenous PRA1 *per se* was responsive to U18666A. The data collectively suggest that the gene encoding PRA1, and those encoding PRA1-affected proteins, potentially encompass response elements for certain transcription factors involved in lipid homeostasis. Consulting the web-based Transcription Element Search System (TESS; <http://www.cbil.upenn.edu/cgi-bin/tess/tess>), we indeed found putative response elements for functionally relevant transcription factors, including sterol regulatory element-binding protein, peroxisome proliferator-activated receptor, and retinoid X receptor, within the promoter of genes encoding relevant proteins (Supplementary Table S7). Sterol regulatory element-binding protein resides in the ER and is activated in sterol-poor conditions by transport to the Golgi complex, where it undergoes proteolytic processing. The processed fragment is then imported into the nucleus, where it switches on the transcription of sterol-regulated gene products that function to increase cellular cholesterol levels (57, 58). On the other hand, peroxisome proliferator-activated receptors are ligand-inducible nuclear hormone receptors, which can be activated by fatty acids and their derivatives (59). Following activation by their ligands and heterodimerization with their obligate partners retinoid X receptor (Supplementary Fig. S2A), peroxisome proliferator-activated receptors interact with the peroxisome-proliferator response

element in the promoter of their target genes and lead to transcriptional regulation of pathways that are involved in lipid metabolism and homeostasis (60–62). Further investigation is needed to clarify how these transcription factors coordinate the expressional regulation of PRA1 as well as its affected proteins, such as LAMC2, ITGA6, ITGB4, CAV1, and FABP5, for adapting to changes in cellular lipid homeostasis.

Concomitant with their elevated expression levels, PRA1 depletion also led to spatial alteration of CAV1, ITGA6 and ITGB4 (Fig. 2B; [Supplementary Fig. S3C](#)), an effect presumably representing increased endocytic/recycling dynamics of alpha6beta4 integrin ([Supplementary Fig. S6](#)). It has been shown that, in the cells with impaired cholesterol export, the Golgi pool of CAV1 is increased, accompanied by cellular cholesterol accumulation at the late endosomes (63, 64). As a constitutive protein of caveolae, CAV1 plays an important role in the regulation of cellular cholesterol homeostasis, and can modulate the activities of other proteins that are involved in such regulation processes (46). While it is unclear whether CAV1 can modulate the function of PRA1 and *vice versa*, the functional link between CAV1 and PRA1 has been suggested by the data that dominant-negative Rab7 and Rab9 can inhibit Golgi targeting of sphingolipids internalized via caveolae (43). Because PRA1 can interact with Rab7 (3) and affect the activity of Rab9 (9), the data implicate that PRA1 and CAV1 may coordinate in regulating lipid homeostasis *via* action of Rabs. Beside its vital role in lipid recycling, CAV1 also regulates integrin endocytosis and cell migration as exemplified by $\alpha 5 \beta 1$ integrin, which can be endocytosed by caveolae in the absence of fibronectin and fibronectin matrix (65). Thus, it is plausible that the increased endocytosis of $\alpha 6 \beta 4$ integrin in PRA1-depleted cells is associated with the increased intracellular pool of CAV1.

The recycling of ITGA6 and ITGB4 is thought to be mediated by Rab11-driven vesicular trafficking, which is increasingly associated with cell migration (66–68) and is important for maintaining cellular cholesterol homeostasis (69, 70). Changes in the cellular level of cholesterol can modulate the intracellular distribution of Rab11 as well as the endocytic routes of a subset of membrane lipids through Rab11 (71). It is conceivable to speculate that the altered distribution of cellular cholesterol by PRA1 depletion (Fig. 5A) may elicit Rab11-dependent pathways, thereby enhancing the efficacy of integrin recycling. In addition, alpha6beta4 integrin associates with vimentin intermediate filaments through the cytoplasmic tail of ITGB4 in a ligand-independent fashion (72). Phosphorylation of vimentin by protein kinase C within the recycling integrin compartment is crucial for the integrin trafficking through the cell (73), and this phosphorylation also regulates vimentin interaction with Rab9 and hence affects intracellular lipid transport (74, 75). A potential interaction between PRA1 and vimentin is revealed by yeast two-hybrid assays (76), indicating a possibility that PRA1 may play a convergent role in lipid transport and integrin recycling

through interacting with vimentin. Additional experiments are required to elucidate better the molecular basis underlying these PRA1-involved processes and the interplay with CAV1.

It has been shown that viruses can hijack the physiological lipid-transfer functions to favor their infections or maintenance (77, 78). In the previous study, we have identified that proper trafficking and full signaling of LMP1 mainly rely on its interaction with PRA1 (16). In this study, we further disclose an association between PRA1 and lipid homeostasis as revealed by the iTRAQ-based quantitative proteomic analysis (Table II; [Supplementary Fig. S2A](#)), reinforcing the view that PRA1 may assist LMP1 in stabilizing into lipid rafts and targeting to destined compartments, by virtue of regulating lipid transport. Conversely, PRA1 interaction with LMP1 can hinder PRA1 from its physical functions, in particular when LMP1 is expressed for long terms or at excessive amounts (Fig. 6). The LMP1-associated sequestration of PRA1 may lead to the functional consequence reminiscent of the effect from PRA1 knockdown (Fig. 6B and C; [Supplementary Fig. S5](#)). In addition, PRA1 is reported to inhibit T-cell factor (TCF)/ β -catenin signaling, which is related to tumorigenesis, by binding to β -catenin and preventing it from translocation into the nucleus (79). LMP1 interaction with PRA1 may hinder PRA1 from binding to β -catenin, thereby allowing nuclear translocation of β -catenin and activation of the signaling. In agreement with this, β -catenin is shown to activate the expression of LAMC2, albeit in colorectal carcinomas (80), suggesting an additional way for PRA1 to affect gene expression. Despite the possibility that other factors may also contribute to the LMP1-associated NPC morphogenesis, the PRA1-involved functions are shown for the first time to be a promoting force in such events.

In conclusion, we discover that PRA1 is involved in lipid homeostasis and cell migration, in aspects of a proteome-wide effect on protein expression and function. We also reveal that EBV-encoded LMP1 may affect these PRA1-involved processes through sequestration of PRA1, coordinating the tumorigenesis of NPC. Because PRA1 is ubiquitously expressed in human tissues, this study will provide a new avenue for exploring the roles of PRA1 in other diseases that are associated with lipid abnormalities, for instance, the type 2 diabetes (58), and neuronal diseases including Alzheimer's disease (81–83).

* The work was supported by grants to Chang Gung University from the Ministry of Education, Taiwan (EMRPD150231; EMRPD170191), a grant to Jau-Song Yu from the National Science Council, Taiwan (Grant NSC 98-2811-B-182-019), and a grant to Yu-Sun Chang from Chang Gung Memorial Hospital (Grant CMRPD150961).

☒ This article contains [supplemental Experimental procedures, Figs. 1–6 and Tables 1–8](#).

‡‡ Both authors contributed equally to this work.

** To whom correspondence should be addressed: Molecular Medicine Research Center, Chang Gung University, 259 Wen-Hwa 1st Rd., Kwei-Shan, Tao-Yuan 333, Taiwan ROC. Tel.: (886)3-2118683; Fax: (886)3-2118683; E-mail: ysc@mail.cgu.edu.tw.

REFERENCES

- Abdul-Ghani, M., Gougeon, P. Y., Prosser, D. C., Da-Silva, L. F., and Ngsee, J. K. (2001) PRA isoforms are targeted to distinct membrane compartments. *J. Biol. Chem.* **276**, 6225–6233
- Figuerola, C., Taylor, J., and Vojtek, A. B. (2001) Prenylated Rab acceptor protein is a receptor for prenylated small GTPases. *J. Biol. Chem.* **276**, 28219–28225
- Bucci, C., Chiariello, M., Lattero, D., Maiorano, M., and Bruni, C. B. (1999) Interaction cloning and characterization of the cDNA encoding the human prenylated rab acceptor (PRA1). *Biochem. Biophys. Res. Commun.* **258**, 657–662
- Seabra, M. C., Mules, E. H., and Hume, A. N. (2002) Rab GTPases, intracellular traffic and disease. *Trends Mol. Med.* **8**, 23–30
- Schwartz, S. L., Cao, C., Pylypenko, O., Rak, A., and Wandinger-Ness, A. (2007) Rab GTPases at a glance. *J. Cell Sci.* **120**, 3905–3910
- Cheng, K. W., Lahad, J. P., Gray, J. W., and Mills, G. B. (2005) Emerging role of RAB GTPases in cancer and human disease. *Cancer Res.* **65**, 2516–2519
- Martincic, I., Peralta, M. E., and Ngsee, J. K. (1997) Isolation and characterization of a dual prenylated Rab and VAMP2 receptor. *J. Biol. Chem.* **272**, 26991–26998
- Hutt, D. M., Da-Silva, L. F., Chang, L. H., Prosser, D. C., and Ngsee, J. K. (2000) PRA1 inhibits the extraction of membrane-bound rab GTPase by GDI1. *J. Biol. Chem.* **275**, 18511–18519
- Sivars, U., Aivazian, D., and Pfeffer, S. R. (2003) Yip3 catalyses the dissociation of endosomal Rab-GDI complexes. *Nature* **425**, 856–859
- Compton, S. L., and Behrend, E. N. (2006) PRAF1: a Golgi complex transmembrane protein that interacts with viruses. *Biochem. Cell Biol.* **84**, 940–948
- Rothman, J. E. (2002) Lasker Basic Medical Research Award. The machinery and principles of vesicle transport in the cell. *Nat. Med.* **8**, 1059–1062
- Chintagari, N. R., Jin, N., Wang, P., Narasaraaju, T. A., Chen, J., and Liu, L. (2006) Effect of cholesterol depletion on exocytosis of alveolar type II cells. *Am. J. Respir. Cell Mol. Biol.* **34**, 677–687
- Evans, D. T., Tillman, K. C., and Desrosiers, R. C. (2002) Envelope glycoprotein cytoplasmic domains from diverse lentiviruses interact with the prenylated Rab acceptor. *J. Virol.* **76**, 327–337
- Simons, K., and Ikonen, E. (1997) Functional rafts in cell membranes. *Nature* **387**, 569–572
- Enouf, V., Chwetozoff, S., Trugnan, G., and Cohen, J. (2003) Interactions of rotavirus VP4 spike protein with the endosomal protein Rab5 and the prenylated Rab acceptor PRA1. *J. Virol.* **77**, 7041–7047
- Liu, H. P., Wu, C. C., and Chang, Y. S. (2006) PRA1 promotes the intracellular trafficking and NF-kappaB signaling of EBV latent membrane protein 1. *EMBO J.* **25**, 4120–4130
- Niedobitek, G. (1999) The Epstein-Barr virus: a group 1 carcinogen? *Virchows Arch.* **435**, 79–86
- Stevenson, D., Charalambous, C., and Wilson, J. B. (2005) Epstein-Barr virus latent membrane protein 1 (CAO) up-regulates VEGF and TGF alpha concomitant with hyperlaxity, with subsequent up-regulation of p16 and MMP9. *Cancer Res.* **65**, 8826–8835
- Kaykas, A., Worringer, K., and Sugden, B. (2001) CD40 and LMP-1 both signal from lipid rafts but LMP-1 assembles a distinct, more efficient signaling complex. *EMBO J.* **20**, 2641–2654
- Gires, O., Zimmer-Strobl, U., Gonnella, R., Ueffing, M., Marschall, G., Zeidler, R., Pich, D., and Hammerschmidt, W. (1997) Latent membrane protein 1 of Epstein-Barr virus mimics a constitutively active receptor molecule. *EMBO J.* **16**, 6131–6140
- Li, H. P., and Chang, Y. S. (2003) Epstein-Barr virus latent membrane protein 1: structure and functions. *J. Biomed. Sci.* **10**, 490–504
- Tsai, C. N., Tsai, C. L., Tse, K. P., Chang, H. Y., and Chang, Y. S. (2002) The Epstein-Barr virus oncogene product, latent membrane protein 1, induces the downregulation of E-cadherin gene expression via activation of DNA methyltransferases. *Proc. Natl. Acad. Sci. U.S.A.* **99**, 10084–10089
- Wu, C. C., Chien, K. Y., Tsang, N. M., Chang, K. P., Hao, S. P., Tsao, C. H., Chang, Y. S., and Yu, J. S. (2005) Cancer cell-secreted proteomes as a basis for searching potential tumor markers: nasopharyngeal carcinoma as a model. *Proteomics* **5**, 3173–3182
- Olsen, J. V., de Godoy, L. M., Li, G., Macek, B., Mortensen, P., Pesch, R., Makarov, A., Lange, O., Horning, S., and Mann, M. (2005) Parts per million mass accuracy on an Orbitrap mass spectrometer via lock mass injection into a C-trap. *Mol. Cell. Proteomics* **4**, 2010–2021
- Griffin, T. J., Xie, H., Bandhakavi, S., Popko, J., Mohan, A., Carlis, J. V., and Higgins, L. (2007) iTRAQ reagent-based quantitative proteomic analysis on a linear ion trap mass spectrometer. *J. Proteome Res.* **6**, 4200–4209
- Bantscheff, M., Boesche, M., Eberhard, D., Matthieson, T., Sweetman, G., and Kuster, B. (2008) Robust and sensitive iTRAQ quantification on an LTQ Orbitrap mass spectrometer. *Mol. Cell. Proteomics* **7**, 1702–1713
- Nesvizhskii, A. I., Vitek, O., and Aebersold, R. (2007) Analysis and validation of proteomic data generated by tandem mass spectrometry. *Nat. Methods* **4**, 787–797
- Mueller, L. N., Brusniak, M. Y., Mani, D. R., and Aebersold, R. (2008) An assessment of software solutions for the analysis of mass spectrometry based quantitative proteomics data. *J. Proteome Res.* **7**, 51–61
- Keller, A., Nesvizhskii, A. I., Kolker, E., and Aebersold, R. (2002) Empirical statistical model to estimate the accuracy of peptide identifications made by MS/MS and database search. *Anal. Chem.* **74**, 5383–5392
- Nesvizhskii, A. I., Keller, A., Kolker, E., and Aebersold, R. (2003) A statistical model for identifying proteins by tandem mass spectrometry. *Anal. Chem.* **75**, 4646–4658
- Khan, A. P., Poisson, L. M., Bhat, V., Fermin, D., Zhao, R., Kalyana-Sundaram, S., Michailidis, G., Nesvizhskii, A. I., Omenn, G. S., Chinnaiyan, A. M., and Sreekumar, A. (2009) Quantitative proteomic profiling of prostate cancer reveals a role for miR-128 in prostate cancer. *Mol. Cell. Proteomics*, Epub ahead of print
- Wang, C. L., Wang, C. I., Liao, P. C., Chen, C. D., Liang, Y., Chuang, W. Y., Tsai, Y. H., Chen, H. C., Chang, Y. S., Yu, J. S., Wu, C. C., and Yu, C. J. (2009) Discovery of retinoblastoma-associated binding protein 46 as a novel prognostic marker for distant metastasis in nonsmall cell lung cancer by combined analysis of cancer cell secretome and pleural effusion proteome. *J. Proteome Res.* **8**, 4428–4440
- Ravn, V., Rasmussen, B. B., Højholt, L., Barfoed, M., Heiberg, I., and Thorpe, S. M. (1993) Reproducibility of subjective immunohistochemical estrogen- and progesterone receptor determination in human endometrium. *Pathol Res Pract* **189**, 1015–1022
- Franz, M., Richter, P., Geyer, C., Hansen, T., Acuña, L. D., Hyckel, P., Böhmer, F. D., Kosmehl, H., and Berndt, A. (2007) Mesenchymal cells contribute to the synthesis and deposition of the laminin-5 gamma2 chain in the invasive front of oral squamous cell carcinoma. *J. Mol. Histol.* **38**, 183–190
- Kato, N., Sasou, S., Teshima, S., and Motoyama, T. (2007) Overexpression of laminin-5 gamma2 chain in clear cell carcinoma of the ovary. *Virchows Arch.* **450**, 273–278
- Lotz, M. M., Nusrat, A., Madara, J. L., Ezzell, R., Wewer, U. M., and Mercurio, A. M. (1997) Intestinal epithelial restitution. Involvement of specific laminin isoforms and integrin laminin receptors in wound closure of a transformed model epithelium. *Am. J. Pathol.* **150**, 747–760
- Rabinovitz, I., and Mercurio, A. M. (1997) The integrin alpha6beta4 functions in carcinoma cell migration on laminin-1 by mediating the formation and stabilization of actin-containing motility structures. *J. Cell Biol.* **139**, 1873–1884
- Cruz-Monserrate, Z., and O'Connor, K. L. (2008) Integrin alpha 6 beta 4 promotes migration, invasion through Tiam1 upregulation, and subsequent Rac activation. *Neoplasia* **10**, 408–417
- Carroll, K. S., Hanna, J., Simon, I., Krise, J., Barbero, P., and Pfeffer, S. R. (2001) Role of Rab9 GTPase in facilitating receptor recruitment by TIP47. *Science* **292**, 1373–1376
- Sincock, P. M., Ganley, I. G., Krise, J. P., Diederichs, S., Sivars, U., O'Connor, B., Ding, L., and Pfeffer, S. R. (2003) Self-assembly is important for TIP47 function in mannose 6-phosphate receptor transport. *Traffic* **4**, 18–25
- Díaz, E., and Pfeffer, S. R. (1998) TIP47: a cargo selection device for mannose 6-phosphate receptor trafficking. *Cell* **93**, 433–443
- Ganley, I. G., and Pfeffer, S. R. (2006) Cholesterol accumulation sequesters Rab9 and disrupts late endosome function in NPC1-deficient cells. *J. Biol. Chem.* **281**, 17890–17899
- Choudhury, A., Dominguez, M., Puri, V., Sharma, D. K., Narita, K., Wheatley, C. L., Marks, D. L., and Pagano, R. E. (2002) Rab proteins mediate Golgi transport of caveola-internalized glycosphingolipids and correct lipid trafficking in Niemann-Pick C cells. *J. Clin. Invest.* **109**, 1541–1550
- Kusakari, Y., Ogawa, E., Owada, Y., Kitanaka, N., Watanabe, H., Kimura,

- M., Tagami, H., Kondo, H., Aiba, S., and Okuyama, R. (2006) Decreased keratinocyte motility in skin wound on mice lacking the epidermal fatty acid binding protein gene. *Mol. Cell. Biochem.* **284**, 183–188
45. Williams, T. M., Hassan, G. S., Li, J., Cohen, A. W., Medina, F., Frank, P. G., Pestell, R. G., Di Vizio, D., Loda, M., and Lisanti, M. P. (2005) Caveolin-1 promotes tumor progression in an autochthonous mouse model of prostate cancer: genetic ablation of Cav-1 delays advanced prostate tumor development in tramp mice. *J. Biol. Chem.* **280**, 25134–25145
 46. Frank, P. G., Cheung, M. W., Pavlides, S., Llaveras, G., Park, D. S., and Lisanti, M. P. (2006) Caveolin-1 and regulation of cellular cholesterol homeostasis. *Am. J. Physiol. Heart Circ. Physiol.* **291**, H677–686
 47. Sparrow, S. M., Carter, J. M., Ridgway, N. D., Cook, H. W., and Byers, D. M. (1999) U18666A inhibits intracellular cholesterol transport and neurotransmitter release in human neuroblastoma cells. *Neurochem. Res.* **24**, 69–77
 48. Soccio, R. E., and Breslow, J. L. (2004) Intracellular cholesterol transport. *Arterioscler. Thromb. Vasc. Biol.* **24**, 1150–1160
 49. Björling, E., Lindskog, C., Oksvold, P., Linné, J., Kampf, C., Hober, S., Uhlén, M., and Pontén, F. (2008) A web-based tool for in silico biomarker discovery based on tissue-specific protein profiles in normal and cancer tissues. *Mol. Cell. Proteomics* **7**, 825–844
 50. Andersson, A. C., Strömberg, S., Bäckvall, H., Kampf, C., Uhlen, M., Wester, K., and Pontén, F. (2006) Analysis of protein expression in cell microarrays: a tool for antibody-based proteomics. *J. Histochem. Cytochem.* **54**, 1413–1423
 51. Ow, S. Y., Salim, M., Noirel, J., Evans, C., Rehman, I., and Wright, P. C. (2009) iTRAQ underestimation in simple and complex mixtures: “the good, the bad and the ugly”. *J. Proteome Res* **8**, 5347–5355
 52. Ikonen, E. (2008) Cellular cholesterol trafficking and compartmentalization. *Nat. Rev. Mol. Cell Biol.* **9**, 125–138
 53. Walter, M., Davies, J. P., and Ioannou, Y. A. (2003) Telomerase immortalization upregulates Rab9 expression and restores LDL cholesterol egress from Niemann-Pick C1 late endosomes. *J. Lipid Res.* **44**, 243–253
 54. Bergo, M. O., and Young, S. G. (2002) Extra Rabs unsharl a lipid traffic jam. *Nat. Med.* **8**, 662–664
 55. Lange, Y., Ye, J., Rigney, M., and Steck, T. (2000) Cholesterol movement in Niemann-Pick type C cells and in cells treated with amphiphiles. *J. Biol. Chem.* **275**, 17468–17475
 56. Palmer, C. P., Mahen, R., Schnell, E., Djamgoz, M. B., and Aydar, E. (2007) Sigma-1 receptors bind cholesterol and remodel lipid rafts in breast cancer cell lines. *Cancer Res.* **67**, 11166–11175
 57. Goldstein, J. L., DeBose-Boyd, R. A., and Brown, M. S. (2006) Protein sensors for membrane sterols. *Cell* **124**, 35–46
 58. Raghoebar, R., Yellaturu, C., Deng, X., Park, E. A., and Elam, M. B. (2008) SREBPs: the crossroads of physiological and pathological lipid homeostasis. *Trends Endocrinol. Metab.* **19**, 65–73
 59. Keller, H., Dreyer, C., Medin, J., Mahfoudi, A., Ozato, K., and Wahli, W. (1993) Fatty acids and retinoids control lipid metabolism through activation of peroxisome proliferator-activated receptor-retinoid X receptor heterodimers. *Proc. Natl. Acad. Sci. U.S.A.* **90**, 2160–2164
 60. Chinetti-Gbaguidi, G., Rigamonti, E., Helin, L., Mutka, A. L., Lepore, M., Fruchart, J. C., Clavey, V., Ikonen, E., Lestavel, S., and Staels, B. (2005) Peroxisome proliferator-activated receptor alpha controls cellular cholesterol trafficking in macrophages. *J. Lipid Res.* **46**, 2717–2725
 61. Fitzgerald, M. L., Moore, K. J., and Freeman, M. W. (2002) Nuclear hormone receptors and cholesterol trafficking: the orphans find a new home. *J. Mol. Med.* **80**, 271–281
 62. Michalik, L., Desvergne, B., and Wahli, W. (2004) Peroxisome-proliferator-activated receptors and cancers: complex stories. *Nat. Rev. Cancer* **4**, 61–70
 63. Garver, W. S., Krishnan, K., Gallagos, J. R., Michikawa, M., Francis, G. A., and Heidenreich, R. A. (2002) Niemann-Pick C1 protein regulates cholesterol transport to the trans-Golgi network and plasma membrane caveolae. *J. Lipid Res.* **43**, 579–589
 64. Cubells, L., Vilà de Muga, S., Tebar, F., Wood, P., Evans, R., Ingelmo-Torres, M., Calvo, M., Gaus, K., Pol, A., Grewal, T., and Enrich, C. (2007) Annexin A6-induced alterations in cholesterol transport and caveolin export from the Golgi complex. *Traffic* **8**, 1568–1589
 65. Shi, F., and Sottile, J. (2008) Caveolin-1-dependent beta1 integrin endocytosis is a critical regulator of fibronectin turnover. *J. Cell Sci.* **121**, 2360–2371
 66. Strachan, L. R., and Condic, M. L. (2004) Cranial neural crest recycle surface integrins in a substratum-dependent manner to promote rapid motility. *J. Cell Biol.* **167**, 545–554
 67. Caswell, P. T., and Norman, J. C. (2006) Integrin trafficking and the control of cell migration. *Traffic* **7**, 14–21
 68. Jones, M. C., Caswell, P. T., and Norman, J. C. (2006) Endocytic recycling pathways: emerging regulators of cell migration. *Curr. Opin. Cell Biol.* **18**, 549–557
 69. Hao, M., Lin, S. X., Karylowski, O. J., Wüstner, D., McGraw, T. E., and Maxfield, F. R. (2002) Vesicular and non-vesicular sterol transport in living cells. The endocytic recycling compartment is a major sterol storage organelle. *J. Biol. Chem.* **277**, 609–617
 70. Hölttä-Vuori, M., Tanhuanpää, K., Möbius, W., Somerharju, P., and Ikonen, E. (2002) Modulation of cellular cholesterol transport and homeostasis by Rab11. *Mol. Biol. Cell* **13**, 3107–3122
 71. Takahashi, M., Murate, M., Fukuda, M., Sato, S. B., Ohta, A., and Kobayashi, T. (2007) Cholesterol controls lipid endocytosis through Rab11. *Mol. Biol. Cell* **18**, 2667–2677
 72. Homan, S. M., Martinez, R., Benware, A., and LaFlamme, S. E. (2002) Regulation of the association of alpha 6 beta 4 with vimentin intermediate filaments in endothelial cells. *Exp. Cell Res.* **281**, 107–114
 73. Ivaska, J., Vuoriluoto, K., Huovinen, T., Izawa, I., Inagaki, M., and Parker, P. J. (2005) PKCepsilon-mediated phosphorylation of vimentin controls integrin recycling and motility. *EMBO J.* **24**, 3834–3845
 74. Walter, M., Chen, F. W., Tamari, F., Wang, R., and Ioannou, Y. A. (2009) Endosomal lipid accumulation in NPC1 leads to inhibition of PKC, hypophosphorylation of vimentin and Rab9 entrapment. *Biol. Cell* **101**, 141–152
 75. Sarria, A. J., Panini, S. R., and Evans, R. M. (1992) A functional role for vimentin intermediate filaments in the metabolism of lipoprotein-derived cholesterol in human SW-13 cells. *J. Biol. Chem.* **267**, 19455–19463
 76. Stelzl, U., Worm, U., Lalowski, M., Haenig, C., Brembeck, F. H., Goehler, H., Stroedicke, M., Zenkner, M., Schoenherr, A., Koeppen, S., Timm, J., Mintzlaff, S., Abraham, C., Bock, N., Kietzmann, S., Goedde, A., Toksöz, E., Droege, A., Krobitsch, S., Korn, B., Birchmeier, W., Lehrach, H., and Wanker, E. E. (2005) A human protein-protein interaction network: a resource for annotating the proteome. *Cell* **122**, 957–968
 77. Tang, Y., Leao, I. C., Coleman, E. M., Broughton, R. S., and Hildreth, J. E. (2009) Deficiency of niemann-pick type C-1 protein impairs release of human immunodeficiency virus type 1 and results in Gag accumulation in late endosomal/lysosomal compartments. *J. Virol.* **83**, 7982–7995
 78. Dreux, M., Dao Thi, V. L., Fresquet, J., Guérin, M., Julia, Z., Verney, G., Durantal, D., Zoulim, F., Lavillette, D., Cosset, F. L., and Bartosch, B. (2009) Receptor complementation and mutagenesis reveal SR-BI as an essential HCV entry factor and functionally imply its intra- and extracellular domains. *PLoS Pathog.* **5**, e1000310
 79. Kim, J. T., Cho, M. Y., Choi, S. C., Kim, J. W., Chae, S. K., Yoon, D. Y., Kim, J. W., and Lim, J. S. (2006) Prenylated Rab acceptor 1 (PRA1) inhibits TCF/beta-catenin signaling by binding to beta-catenin. *Biochem. Biophys. Res. Commun.* **349**, 200–208
 80. Hlubek, F., Spaderna, S., Jung, A., Kirchner, T., and Brabletz, T. (2004) Beta-catenin activates a coordinated expression of the proinvasive factors laminin-5 gamma2 chain and MT1-MMP in colorectal carcinomas. *Int. J. Cancer* **108**, 321–326
 81. Karten, B., Campenot, R. B., Vance, D. E., and Vance, J. E. (2006) The Niemann-Pick C1 protein in recycling endosomes of presynaptic nerve terminals. *J. Lipid Res.* **47**, 504–514
 82. Koh, C. H., and Cheung, N. S. (2006) Cellular mechanism of U18666A-mediated apoptosis in cultured murine cortical neurons: bridging Niemann-Pick disease type C and Alzheimer’s disease. *Cell. Signal.* **18**, 1844–1853
 83. Liu, J. P., Tang, Y., Zhou, S., Toh, B. H., McLean, C., and Li, H. (2009) Cholesterol involvement in the pathogenesis of neurodegenerative diseases. *Mol. Cell. Neurosci.*, Epub ahead of print